Spring 1-1-2017

A Study on Crystallization Kinetics Using Steady State CSTRs

Sankaranarayanan Ayyakudi Ravichandran
University of Colorado at Boulder, sankar.bharghav@gmail.com

A study on crystallization kinetics using steady state CSTRs

By

Sankaranarayanan Ayyakudi Ravichandran

BTech. Chemical Engineering, Anna University (India), 2015

A Report submitted to the
Faculty of the Graduate School of the
University of Colorado in partial fulfillment
of the requirements for the course of
Master's Thesis
Department of Environmental Engineering
2017

This thesis entitled:

Study on crystallization kinetics using steady state CSTRs

Written by

Sankaranarayanan Ayyakudi Ravichandran

Has been approved for the Department of Environmental Engineering

_____

(Professor John Pellegrino, Department of Mechanical engineering)

_____

(Professor Joseph Ryan, Department of Environmental Engineering)

_____

(Professor R. Scott Summers, Department of Environmental Engineering)

*Date*_____

The final copy of this thesis has been examined by the signatories, and we find that both the content and the form meet acceptable presentation standards of scholarly work in the above-mentioned discipline.

Abstract

Ayyakudi Ravichandran, Sankaranarayanan

(MS, Department of Environmental Engineering)

Study on crystallization kinetics using steady state CSTRs

Thesis directed by Professor John Pellegrino

This research focuses on developing techniques to reliably analyze the crystallization kinetics of sparingly soluble salts in reject/concentrate streams from membrane-based, inland water supply processes. More usable water can be recovered (and lower disposal costs incurred) from these concentrate streams through efficient crystallization. Currently, pellet softening is a preferred mode of crystallizing the supersaturated salts from such streams. A conventional pellet softener in the ideal sense is a non-ideal plug flow reactor (PFR). In this work, we present the evolution of a steady state, continuously stirred tank reactors (CSTRs)-in-series approach, to approximate a PFR, to study crystallization kinetics of a model solution that is supersaturated in calcium carbonate. Furthermore, using this setup, we can systematically study crystallization, in general, and develop quantitative engineering-design, scale-up parameters. In the current work, we have used pH, conductivity and turbidity changes in the system to monitor crystallization in the CSTRs-in-series setup. We have used up to six CSTRs with individual residence times of approximately 2, 5 and 11 min. This system operates in a steady state mode with total treatment times between ~15-68 minutes. Our reactor setup was capable of handling up to 875 mL/min of hard water at the shortest residence time studied. The supersaturation was depleted ~25% with a total reactor residence time of 15 min and over 50% for overall times in the range of ~68 min. We have also been able to estimate induction times for crystallization based on the metric of 5 NTU as being the point of discernible crystal formation. Interestingly, crystallization always began in the second tank for all

the residence times. Thus, the induction time appears to be influenced by other process variables beyond simply the time spent (by the inlet water) in the first tank of the CSTRs-in-series setup. Our initial hypothesis is that the induction time depends on the level of mixing in the first reactor stage and screening\studies of this variable are presented and discussed, but significant further work is needed.

Acknowledgements

I thank Dr. John Pellegrino for providing me the opportunity to do research under his guidance and for his constant support. I would like my thank my family and especially my mother for being a constant source of inspiration. I thank Mr. Saied Delagah of the Bureau of Reclamation for supporting our research. This research would not have been possible without the diligence and hard work of Ms. Dakota Edwards, Ms. Erika King and Ms. Jordan Krist. I would also like to thank Mr. Suroj Lamichhane, Ms. Kaitlyn Tedesco and Mr. Michael Trezek for the background work. I thank Mr. Jacob Hutfles for the many interesting scientific conversations. I thank Dr. Fredrick Luiszer for the ICP-OES analysis. I would also like to express my sincere gratitude to Professor Joseph Ryan and Professor R. Scott Summers for consenting to be a part of my committee.

Table of contents

List of figures

List of tables

Chapter 1

1.1 Introduction

The present study is an attempt to understand calcium carbonate ($CaCO_3$) crystallization kinetics to aid optimization of membrane water treatment processes. The precipitation of $CaCO_3$ from supersaturated solutions has been widely investigated by various researchers [1-4]. The precipitation of $CaCO_3$ from electrolyte solutions containing calcium ions has been explained previously by the classical mechanisms of crystallization. The classical view of nucleation envisages a surface-controlled precipitation of solids from a supersaturated solution. The first stage is the formation of these initial crystals or nuclei. Nucleation can be caused by the presence of surfaces; foreign particles or seed crystals. Nucleation itself can be of two types, primary nucleation and secondary nucleation. Primary nucleation and secondary nucleation refer to crystal formation in the absence and presence of surrounding crystal particulates. Primary nucleation can either be homogeneous (no foreign seed particulates) or heterogeneous (crystallization induced by foreign particulates) [5]. More recent studies have suggested that the precipitation of $CaCO_3$ could involve mechanisms that are not fully explained by these classical mechanisms [6-8]. The crystallization process has been shown to follow pathways that involve amorphous calcium carbonate pre-nucleation precursors (ACC) [9,10]. Studies of crystallization precursors using cryo-TEM have shown that the ACC have sizes on the order a few nanometers [7].

1.2 Pellet softening

Pellet softening is a method of water treatment to remove hardness. Pellet softeners are essentially fluidized bed columns that contain particulates such as sand (to enhance surface area) for the removal of sparingly soluble salts from water such as calcium and magnesium carbonates. In traditional pellet softening process, supersaturated feeds are dosed with alkali to lower pH to favor precipitation demineralization and fed to pellet softeners. Softeners are designed in such a manner that seed particulates and crystals are fluidized. Periodically pellet softeners are stopped from operating and the precipitated salts are removed. From a chemical engineering perspective, pellet softeners are akin to a fed-batch, non-ideal plug flow reactor (PFR). In crystallization parlance, seed particulates can be considered as catalysts. Though crystallization does not involve actual chemical reactions, the addition of seed particulates enhances the surface area available for crystallization; can increase the kinetics; and the seed particulates themselves remain unchanged during the entire process. One of the fundamental goals of this project is to devise engineering design criteria for pellet softener reactor design. The fluidization height depends on the flux required, the number density of seeding particulates, bed porosity and velocity of flow of liquid in the reactor. It is important to note that in cases where the inlet stream is dosed with alkali, to speed up the precipitation process further, the exit stream from the pellet softener is also supersaturated on account of high pH levels, i.e. over softening. Thus, in many cases the treated water is mixed with an inlet water bypass and/or is acidified [11]. Figure 1 shows the schematic of a pellet softener, the schematic is adapted from Scaghen et al [11].

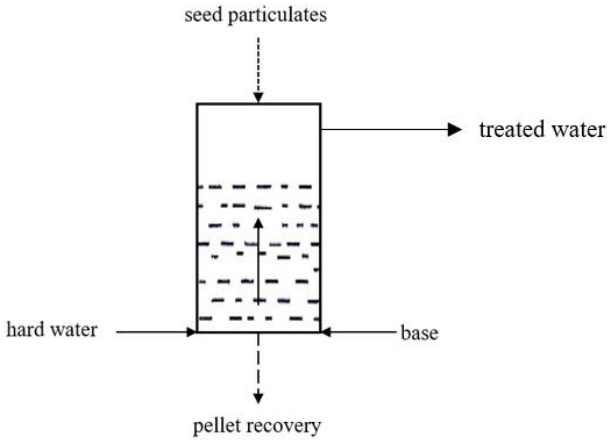

Figure 1- Schematic of pellet softener

The initial addition of base and subsequent neutralization using acid can prove to be operationally problematic from a process perspective due to additional disposal and consumables' costs. Moreover, the addition of chemicals (lime) to increase the pH results in more calcium entering the system; precipitating out; and adding to the volume of solids that require disposal. If this chemical addition can be eliminated from pellet softening, this could prove to be beneficial from a process engineering perspective as two unit processes are eliminated, the addition of lime to increase pH and addition of acid to increase the pH subsequently.

1.3 Significance of research

Membrane processes involve sending the feed stream through membrane modules and collection of treated water that permeates. The remainder is a concentrate stream (the feed that doesn't permeate). The management of concentrate streams is a serious challenge in terms of disposal in an environmentally sustainable manner. The concentrate stream can be theoretically minimized by increased recovery of useable water from the feed, or further processing of the concentrate to recover water. The deposition of scale-forming compounds such as $CaCO_3$ limits the maximal recovery of useful water through the membrane. The precipitation of $CaCO_3$ from supersaturated process water can foul the membrane and reduce the overall flux of the system and durability of

the membrane. An interesting concept termed intermediate concentrate demineralization (ICD) has been studied previously by researchers. The process involves treating the feed water to the extent that the supersaturation and scaling characteristics of the feed water permits and then subjecting the concentrate stream to an intermediate treatment, i.e. ICD. It has been previously established that the possibility of $CaCO_3$ precipitation through alkali-induced precipitation techniques is a viable ICD method [12]. The removal of ions in the form of $CaCO_3$ could also theoretically reduce the propensity of forming calcium sulfate ($CaSO_4$) precipitate, another key membrane scaling agent. Increased sulfate concentration is known to decrease the rate of $CaCO_3$ precipitation to a certain extent [13].

1.4 Initial work

This section of the chapter deals with prior work done by our group and are foundational to the work that will be discussed in further chapters [14]. Specific details on pH, conductivity and turbidity measurements are provided in Chapter 2.

1.4.1 Preliminary studies measuring crystallization kinetics

The group had initially used the composition of a concentrate water produced at a treatment plant trial in Brighton, CO (Table 1). They had also modelled an electrolyte system to study crystallization of sparingly soluble salts, more specifically, $CaCO_3$. The electrolyte system in question was closely modelled on the reject water stream obtained from that treatment facility in Brighton, CO. Aqueous electrolyte thermodynamics software (OLI stream analyzer) was used to arrive at the composition of the electrolyte system. The constituent salts of the system are Na_2SO_4, $NaHCO_3$, $CaCl_2$ and $MgSO_4 \cdot 7H_2O$. Initial studies were conducted in batch mode.

Table 1- Composition of model electrolyte system. [14]

salt	**concentration (g/L)**
calcium chloride	1.4760
magnesium sulfate (heptahydrate)	1.2078
sodium bicarbonate	1.5624
sodium sulfate	1.5624
silica	0.0601

1.4.2 Prediction of equilibrium

The thermodynamic equilibrium. conditions of the electrolyte system in question were predicted across various temperatures using OLI Stream analyzer software. Further the pH and temperature dependence of carbonate equilibria adds another layer of complexity to the stochastic nature of crystallization. The final composition of the solution at equilibrium in terms of mass of $CaCO_3$ precipitate are shown in Figure 2. Thus, in the next stage of batch experimentation, the researchers devised a technique to overcome the problem of dissolving salts in water, all at once, to create a state of supersaturation.

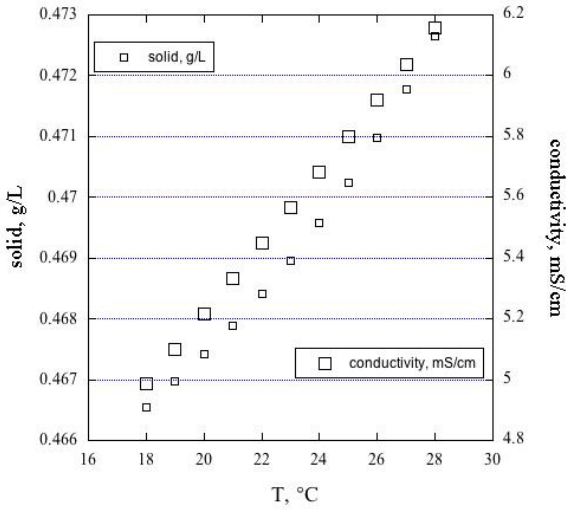

Figure 2- Mass of precipitate (g/L) at equilibrium vs. temperature (pH is ~ 8 at equilibrium).

Initially the researchers attempted to mix all the salts, which constituted the model electrolyte, in water at once and then stir the mixture to analyze the crystallization process. The kinetics of the crystallization process was sensed using turbidity and conductivity. As the crystallization proceeds the conductivity of the solution initially increases as the dry salts dissolve into solution and then decreases as crystallization results in a decrease in the concentration of ions. Further turbidity measurements increased as more crystals are formed. One of the primary motives of these experiments was to estimate the induction time. Induction time is the lag phase between achieving supersaturation and the initial appearance of discernible crystals. The adding of dry salts into the water at once and stirring them was not found to be an effective method to study crystallization kinetics by the researchers. The dry salts required about 3 minutes to dissolve in water completely. The dynamic process of salt dissolution created enough background noise to make effective measurements of crystallization kinetics problematic. There was difficulty in estimating induction time reliably and in a reproducible manner across replicates.

Crystallization occurs due to the interaction of sodium bicarbonate and calcium chloride. The other two salts present in the model solution being sodium sulfate and heptahydrate of magnesium sulfate. Thus, instead of mixing all the constituent salts at once two different unsaturated electrolyte solutions were prepared. The two electrolyte solutions in question are referred to as solution 1 (calcium chloride and heptahydrate of magnesium sulfate) and solution 2 (silica, sodium bicarbonate and sodium sulfate) in further sections. Their compositions are listed in Table 2. The researchers used two electrolyte solutions of this type to conduct future experiments.

Table 2- Composition of binary electrolyte system. [14]

component	solution 1 (g)	solution 2 (g)
calcium chloride	1.4760	
magnesium sulfate (heptahydrate)	1.2078	
sodium bicarbonate		1.5624
sodium sulfate		1.5624
silica		0.0601
water	500	500

They also observed that conductivity is quite sensitive to changes in ambient temperature during the crystallization process. Also, it was observed that the equilibrium conductivity value of 5.44 mS/cm was not observed during the reaction time studied. (In the case of crystallization reaction time implies crystallization time.) This could have meant that the equilibrium was not reached or changes in temperature could have altered the conductivity at equilibrium. It was also observed by the researchers that the silica present in solution 2 did not completely dissolve into solution in a reasonable period of time and remained suspended in solid form.

1.4.3 Experiments mixing two electrolyte solutions

The electrolyte system (solution 1 and 2) was mixed in plastic beakers equipped with a stirrer setup. Initially 500 mL of solution 1 was stirred in beakers and solution 2 was rapidly added to it. The experiments were run simultaneously across six replicates. Two types of experiments were performed, with and without stirring. It was observed that the crystallization process in the case of stirring was much faster than in the case of experiments run without stirring. In the case of trials run without stirring, crystallization was observed 25-30 minutes after the electrolytes were mixed.

An interesting observation was made with regards to turbidity trends in stirred and non-stirred modes of batch experiments. The plots of turbidity and conductivity versus reaction time are shown in Figure 3.

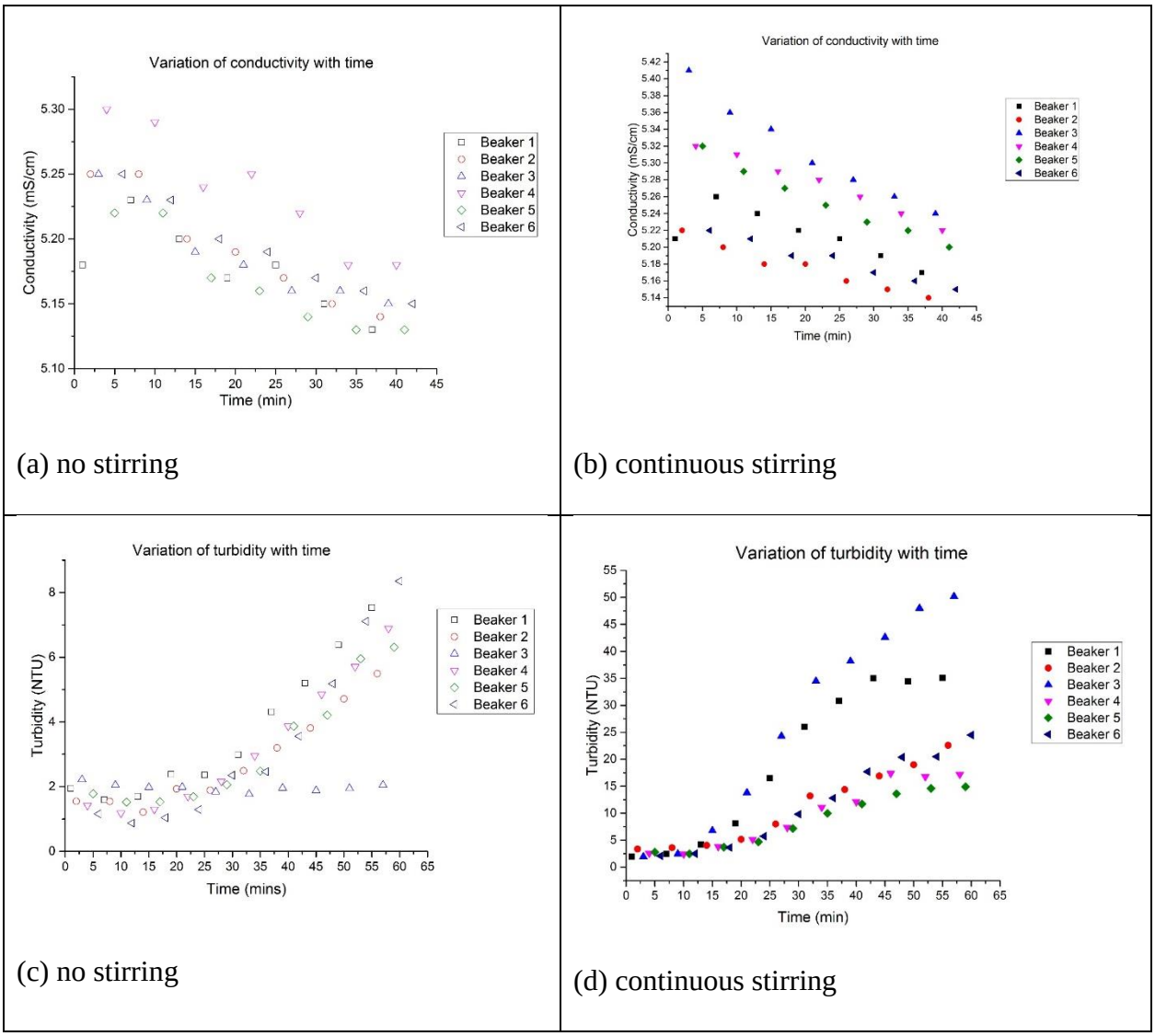

Figure 3- Plots of turbidity and conductivity versus time for continuous stirring and no stirring modes of experiments. [14]

It could be speculated that there was some extent of settling of particulates during crystallization in the absence of stirring and this could have resulted in decreased levels of turbidity being measured. Conductivity data collected from experiments that were being stirred showed a larger

spread than trials performed without stirring. It was reported that the investigators tried to take conductivity measurements consistently from particular regions of the jars (left corner, right corner, etc.) so the variability could be related to the mixing inhomogeneity that existed.

1.4.4 Aeration experiments

Two types of bubble aeration were examined to assess whether or not crystallization was significantly influenced by this process for any reason (e.g. sweeping CO_2, adding surface area, or mixing). A single open tube and hydrophobic, microporous, polypropylene membranes were used for aerating the crystallizing solution. The details regarding the preparation of hollow fiber membrane devices (HFM) are explained in detail in Chapter 2. The HFM devices used are shown in Figure 4.

Besides using HFM, aeration was also carried out using a plain plastic tube (henceforth referred to as plain bubbling). The plots of conductivity and turbidity vs time for aeration experiments without stirring are shown in Figure 5 [14].

Figure 4- HFM aeration device and plain bubbling tube. [14]

Developing equivalency of conditions for the two methods was elusive. Nonetheless, nominal parameters were as follows. The air flow rate in the case of plain bubbling and HFM bubbling was 170 mL/min for each tank. The pressure in the air lines in the case of HFM bubbling was 8 psig

and in the case of plain bubbling the pressure was negligible. Turbidity formation was observed visually in both cases about 20-25 min into the experiment. The bubbles through HFM aeration were more in number and smaller in size than when compared to bubbles produced through plain bubbling. The bubble size in the case of HFM bubbling was approximately 1.5 mm and in the case of plain bubbling was 6 mm as reported by the investigators.

The turbidity at the end of 60 min was between 20-41 NTU (nephelometric turbidity units) across simultaneous replicates for membrane bubbling whereas for plain bubbling turbidity was between 43 to 62 NTU. The researchers also interestingly noted that the turbidity values had a greater spread in the case of HFM bubbling than plain bubbling. The researchers speculated that this could be due to the dynamic effect the HFM bubbles owing to their high surface to volume ratio. Another interesting observation made by them was that the conductivity of the crystallizing solution at equilibrium was lower in the case of plain bubbling when compared to HFM bubbling (5-5.05 mS/cm versus 5.15-5.2 mS/cm).

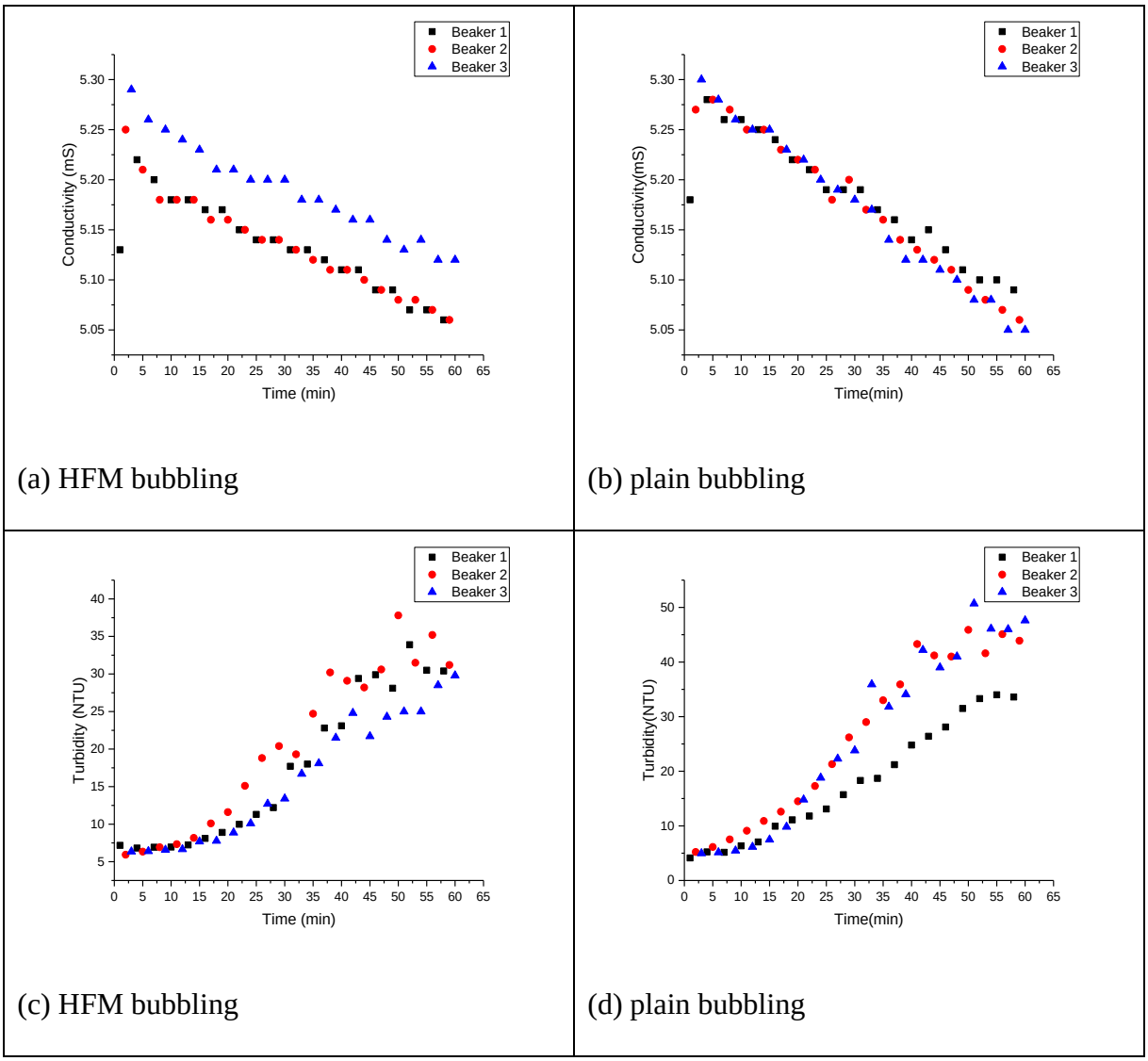

Figure 5- Conductivity and turbidity against time for aeration experiments. [14]

The group observed that as the crystallization proceeded, the pressure drop across the air lines supplying air to the HFM bubbling devices increased. This was rationalized to be due to the deposition of crystals onto the HFM strands. The researchers attempted to discern any influence between the flow rate of air and crystallization. Experiments were performed with two different flowrates. The air flowrates to two jars run simultaneously were 369 mL/min and 451mL/min, respectively. Aeration with 7 or 10 fibers HFM loops and or plain bubbling were used. For flowrate corresponding to 451 mL/min a pronounced change in conductivity was observed. The initial

conductivity was between 5.25-5.3 mS/cm in the case of experiments for both levels of flow. The experiments were run for about 60 min. The researchers observed that the slope of conductivity decrease was greater for plain bubbling at the higher flowrate (451 mL/min) and at the end of 60 min reaches a low value of conductivity (~5.03 mS/cm). In the case of the lower flowrate the conductivity reached a value of ~5.07 mS/cm. In the case of HFM aeration performed with a seven strand HFM, the slope of conductivity decrease was lower for 7 fibers at the higher flowrate when compared to trials performed with the lower flowrates. The researchers observed that the use of HFM aeration showed that apparent crystallization didn't reach completion within first 60 min of experiment. In the case of 7 fiber HFM at the higher flowrate the researchers observed a much higher spread in data. Plots for conductivity and turbidity vs. time showing variation in kinetics between flow rate (22 and 44 flow meter setting) for both HFM and plain bubbling are shown in Figure 6 and Figure 7, respectively. The researchers speculated that this could be the effect of different bubble sizes at higher flowrates. At higher flowrates the number and size of bubbles are very varied, this could potentially influence spatial variance in conductivity data in the jar. No stirring was applied during the aeration experiments the investigators speculated that the differential mixing effects of 7 fiber HFM, 10 fiber HFM and plain bubbling could also influence the spread in the data, especially conductivity. In conclusion, the air flow had a greater effect on crystallization kinetics than the number of fiber strands in the HFM. Higher flowrates contributed to larger spreads in turbidity data and this may be speculated to be due to variable bubble geometry and number density.

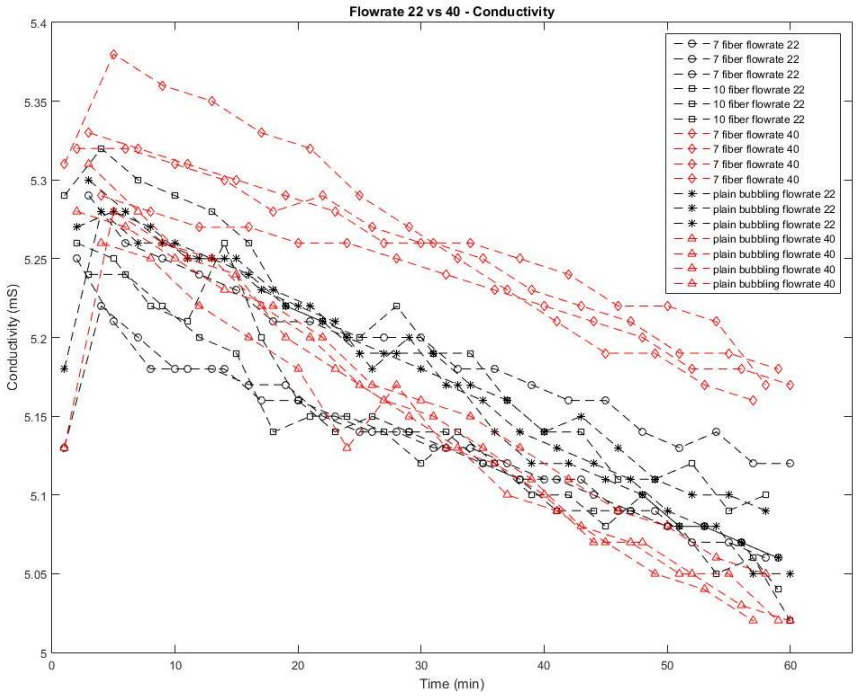

Figure 6- Conductivity vs. time showing variation with flowrate (all flowrate experiments HFM and plain bubbling). [14]

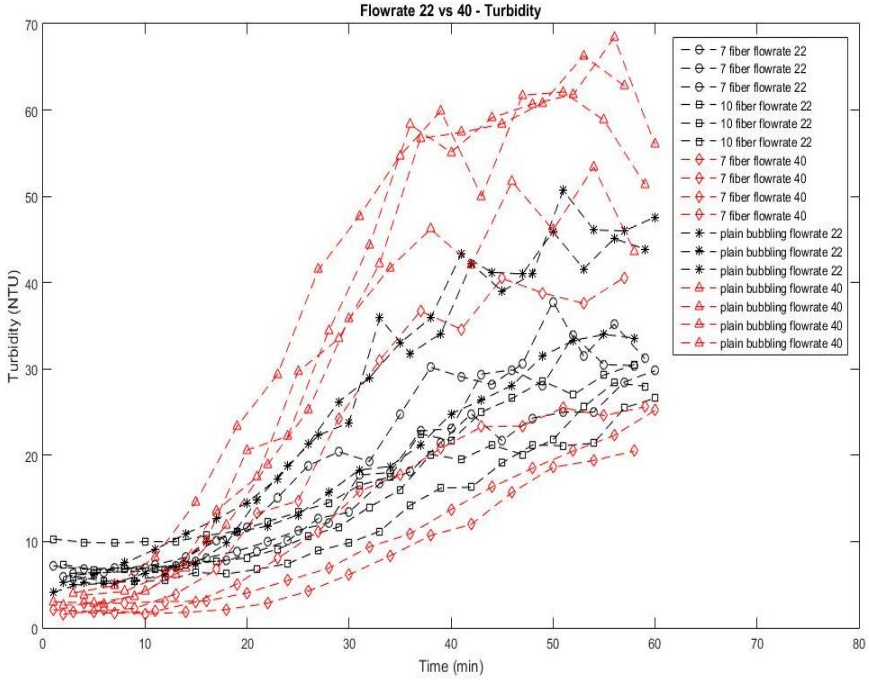

Figure 7- Turbidity vs. time showing variation with flowrate (all flowrate experiments HFM and plain bubbling). [14]

1.5 DI water tests

As a control, the investigators studied the impact of aeration on the deionized (~18 MΩ·cm, aka DI) water conductivity and pH. Each jar was individually filled with 1 L of DI water and connected to the main air outlet. Conductivity was measured in the front left corner of the jar while pH in the front right corner of the jar for sake of consistency keeping in mind the spatial variance of the said measurements. Both probes were rinsed in still DI between measurements. A timer was started as the first jar was filled with DI water the control jar was poured first. The t = 0 reading for the control was measured 150 s after the jar was filled. The test jar was filled with DI water 30 s after the control. The t = 0 reading was taken 2.5 min after DI water was poured (this is 3 min after the control was poured). The test timer was started at this time. No air was supplied to the test until the timer was started so the t = 0 reading was in still water for both jars. The DI water was aerated using open bubbling; and 10 and 7 strand HFM. Different back pressures and flow rates were used across trials. The control was exposed to the ambient conditions in the lab. No stirring was applied to the control. Open bubbling was applied approximately 1" from the bottom of the jar, the flexible nature of the HFM did not permit accurate and consistent positioning. The control and test jars were run concurrently. Test jar readings taken every min and control readings every 30 s starting at t = 0. All experiments were conducted in 17-19°C temperature range. The results from these trials are tabulated in Table 3.

Table 3- Overall factor/level combinations and nominal changes in conductivity and pH over 1 h period for DI water experiments [14].

aeration method	flowmeter setting (mm)	[1]P (psig)	[2]flowrate (mL/min)	[3]jar #1	jar #2	jar #3	jar #4	jar #5	jar #6
[4]calibration no flow	NA	NA	0	-0.01 -3.46	0.64 -3.97	-0.24 -3.5	-0.13 -3.38	0.64 -2.8	-0.56 -3.57
open tube	15		842	-0.4 -3.9	0.4 -2.6	0.4 -2.8	0.8 -2.5	0.9 -2.7	-0.7 -2.2
open tube	10		630	-0.6 -2.9	0.9 -2.6	0.6 -3.4	0.8 -1.1	1.7 -2.3	-2.3 -2.1
7-fiber HFM	10	5	451				-1.6 -2.2		
7-fiber HFM	16	10	403	-1.1 -2					
7-fiber HFM	10	16	369						-2.4 -2.4
open tube	5		360	0 -3	1 -3.1	1 -1.9	0.9 -2.3	-3.4 0.8	0.4 -3.8
7-fiber HFM	15	11	325		-0.8 -3.5				
7-fiber HFM	10	7	234	-2.3 -2.7					
10-fiber HFM	10	7	234					-0.7 -2.7	
7-fiber HFM	5	4	170				-1.6 -0.5		-2.9 -2.2
7-fiber HFM	5.5	5.5	160			-1.7 -2.9			
7-fiber HFM	11	10	148					0.5 -3.2	
7-fiber HFM	9	9	82		-0.2 -2.3				
10-fiber HFM	5	5.5	76	0 -2.5			0 -2.9		
7-fiber HFM	10	9	70			-2.2 -3.9			
10-fiber HFM	10	9	70				-0.3 -3		
10-fiber HFM	5	7	10.7						-0.5 -2.5
10-fiber HFM	10	10	9.3	-0.2 -0.2					-0.7 -2.8
7-fiber HFM	6	7	7					0.7 -2.4	
10-fiber HFM	5	6	6.9			-0.1 -1.7			
10-fiber HFM	10	13	1.4			-1.2 2.8			
10-fiber HFM	9	11	1		0.9 -3.5				
10-fiber HFM	5	10	0.9		0.9 -2.9				
10-fiber HFM	5	11	0.7					1.7 -2.5	

[1]measured by in-line pressure gauge between rotameter and jar [2]interpolated from prior calibration results [3]for all jars, top number is conductivity change in µS/cm and bottom number is change in pH [4]average of 7 separate measurements run concurrently with each bubble introduction method [14].

All these experiments show a decline in pH. This would be expected as the water equilibrates with CO_2. Moreover, a strong relationship could not be established between conductivity and CO_2 absorption. As CO_2 equilibrates with water carbonate equilibria should set in in the water and theoretically CO_3^{2-} and HCO_3^- must also be present. The investigators did not measure any significant values of conductivity, this points to a possibility where the conductivity instrumentation does not have the requisite resolution to capture the response due to carbonate equilibria. The conductivity measurements obtained could be due to noise associated with the instrumentation.

1.6 Conclusions

The investigators, Dr. John Pellegrino (PI) and his team of undergraduate researchers evolved a methodology by way of simulating supersaturated solutions by means of combining 2 electrolyte solutions. Initial scouting work on crystallization kinetics threw light on various parameters that could be used to measure the kinetics of crystallization, viz., conductivity and turbidity. The effect of various modes of aeration and background studies on aeration effect of DI water was also studied. The challenges with these experiments include large spreads of data collected over replicates, difficulty in controlling air flowrate and spatial spread of conductivity values in jars. A better experimental protocol was needed in order to identify whether or not changes in process variables affected the crystallization kinetics versus simply providing responses within the inherently stochastic kinetics of crystallization.

Chapter 2

2.1 Measurement of turbidity, conductivity and pH

An Ecosense EC300 meter was used to measure conductivity and Denver Instrument model 220 was used for measuring pH. Turbidity measurements were taken with a sample of ~15 mL from the reactor in a cuvette and measuring the turbidity using a Hach 2100Q turbidimeter. After measuring the turbidity, the solution from the cuvette was transferred back to the beaker in the case of batch experiments and in the case of steady state experiments the solution in the cuvette was discarded after measurement was made.

2.2 Preparation of hollow fiber membrane (HFM) devices

Strands of hollow fiber membranes (HFM) were looped to make the aeration device. Seven to 10 strands of hollow fiber, microporous (~0.2 micron pores), polypropylene membranes with lengths 7-8 in were cut to length. The strands were then carefully bent in a manner that there was no sharp bends nor breakage in the membrane strands. The bending was such that the open ends of all the membranes faced to one direction. A 2 in length and ¼ in diameter rigid plastic tubing was slid over the open end of the membrane. The membrane was held in place by the rigid tubing using a two-part epoxy. The epoxy is then allowed to cure for 8-12 h and then a small section of the tubing is cut off radially to expose the open HFM ends. The HFM devices were then inserted into one-holed rubber corks that were then mounted into holes on the faces of the beakers. The aeration line is then attached to the other end of the hole present in the one holed cork (the rubber cork mounts to the hole in the wall of the jar and the hole in the cork holds the HFM device and aeration tube in place).

2.3 Experiments

2.3.1 General procedure for steady state experiments

The experimental set up incorporates a Philips and Bird stirrer setup (with six stirrers) and a set of six acrylic jars. Peristaltic pumps (Masterflex) equipped with appropriate tubing as per required flowrate were used to transfer the crystallizing liquor from one continuous stirred tank reactor (CSTR) to another. The volume in each CSTR was maintained using a dynamic weir system. The suction ends were placed at a certain height from the base of the reactor so that the pumps lift the liquid only after a certain volume has been reached in a particular CSTR. Solutions 1 and 2 were pumped into the first reactor using peristaltic pumping. The pH, conductivity and turbidity readings were taken after the CSTR-in-series system reaches steady state., that is, after the last CSTR operation time reached beyond stabilization time t_s. Detailed explanation on stabilization time is provided in section 4.1. The pH, conductivity, and turbidity readings were taken in replicates at least twice with a minimum time interval of 30 min between two sets of readings, after steady state was reached. The schematic of the reactor is shown in Figure 8. Figure 9 shows the CSTR during operation. The overall process flow sheet of CSTRs-in-series experimental setup is shown in the appendix (appendix A).

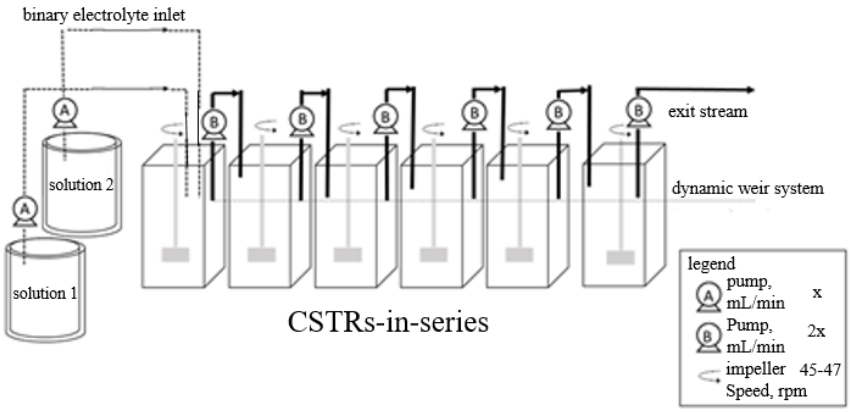

Figure 8- Schematic representation of CSTRs-in-series setup.

Figure 9- Six CSTRs running in steady state (individual residence time, τ = 11.3 min).

2.3.2 Study on the effect of aeration

Continuing in the vein of the preliminary experiments, mentioned previously, further evaluations were conducted to introduce air bubbles using hollow fiber membranes (HFM) and through a 1/8” tubing to create bubbling as a "sort-of" control, in this newly-adopted, steady-state protocol. The bubbles that result from aeration could make available more surface area. Moreover, the HFM by itself could present more surface area inside the crystallizer. The increased surface area could then act as nucleation sites for crystallization. Previously researchers had studied through experimentation and modelling the effect that aeration has on removing CO_2 from the crystallizing liquor. The rationale was that the process of aeration could alter the CO_2 dynamic balance within the fluidized reactor that was used in those studies [22] [23]. This may be unlikely in the case of our experiments due to the at low air flowrates used. Nonetheless, any and all of these effects could all result in faster crystallization. If the CO_2 mass transfer favors a liquid to gas transfer of CO_2, then the pH of the crystallizing solution increases. The increase in pH levels due to this phenomenon would improve the rate of crystallization.

2.3.3 Plain bubbling and HFM aeration experiments

HFM aeration experiments were carried out utilizing 5-6 CSTRs-in-series. The first reactor of the six CSTRs-in-series setup was supplied aeration through an HFM aeration device and a 1/8" tube (plain bubbling). The air was supplied using peristaltic pumps, open to the atmosphere on the intake end, and the flowrate was monitored using a digital air flow meter (Omega, FMA-A2302). Turbidity, pH and conductivity readings were collected from each of the CSTRs-in-series after the reactor system reached steady state. Then the air flow was started after the steady-state was reached. The reactor system was then allowed to reach steady-state again, at which point, turbidity, pH and conductivity readings were taken.

2.3.4 Precipitate collection experiments

Experiments were performed to analyze the amount of $CaCO_3$ crystals precipitated after the supersaturated solution was processed by the CSTRs-in-series reactor configuration. The measuring of the mass of crystals collected would allow us to quantify the extent of supersaturation exhausted during the time it spent in the reactor. A broad objective is to observe if there is a stable and reproducible correlation between turbidity readings and actual mass of crystals collected at the end of the reaction process i.e. from the last CSTR in the CSTR-in-series setup.

The precipitate was collected after the system reached steady-state. About 1.3 to 1.8 L of liquor from the 6^{th} tank in the CSTRs-in-series reactor configuration was siphoned off by a peristaltic pump and pumped across a 0.2 µm ePTFE filter (Donaldson AX09-059) encased in an acrylic membrane cross-flow cell. The permeate was carefully collected in a vessel connected to a vacuum suction (it is important to note that the ePTFE membrane had a high degree of hydrophobicity and needed to be pre-wetted in isopropanol so that water may transit through the membrane easily after solvent replacement). The membrane was previously pre-weighed and the weight recorded. The

membrane with the $CaCO_3$ precipitate was dried overnight and the weight of the membrane and precipitate was measured and thus the weight of $CaCO_3$ per liter of permeate was ascertained. Some of the selected permeate streams were also sent for ICP-OES (inductively coupled plasma optical emission spectrometry) analysis to measure the concentration of Mg^{2+} and Ca^{2+} ions.

2.3.5 Residence time distribution (RTD) experiments

To get a measure of the non-ideal behavior of the CSTRs-in-series reactor configuration residence time distribution tests were carried out. The reactors were arranged in a single CSTR configuration, then a two-CSTRs-in-series configuration, and so on, until the six-CSTRs-in-series configuration. Tracer tests were carried out for each of these configurations because it is easier to accurately sample the exit stream of the final tank in a series, than each of the tanks individually for a six-CSTRs-in-series setup. The reactors were pumped with DI water with a flowrate such that the theoretical residence times of 2.4 and 5.2 min was maintained for each CSTR. Then a pulse input of 10 mL NaCl solution (180 g/L) was injected into the first reactor. The response was observed by measuring the conductivity of the outlet stream from the final CSTR in the series. The conductivity of the outlet streams was continually logged by an Orion Vstar conductivity probe and meter with an automatic temperature controller. Previously, a conductivity versus concentration of NaCl calibration curve was obtained. Using the calibration curve, and the conductivity response from the CSTRs-in-series setup, concentration versus time curves were obtained for one, two, three, etc. CSTRs-in-series. The exit age distribution function was then obtained from the concentration versus time curves.

Chapter 3

3.1 Introduction

In this chapter, experiments have been performed in batch mode to study crystallization kinetics and the effect of aeration on DI water controls' pH and conductivity. In general, a significant change over previous experiments was that the volume of liquid in each of the jars used to perform the experiments was increased from 1 to 2 L. Studies were performed to measure crystallization kinetics in the presence and absence of silica in solution 2. Moreover, we evaluated in-situ and 'grab' sampling techniques for pH and conductivity measurements during crystallization trials in order to achieve less variability.

3.2 Background study on aeration

It was observed that the increase in the volume of liquid in the reactor from 1 to 2 L allows for better exposure of liquid to bubble surfaces (Figure 10). Experiments were conducted in batch mode to observe the effect of aeration on pH. Acrylic jar test beakers with 2 L of DI water were supplied air through hollow fiber membranes, and the pH was continually measured. The air flow rates were in the range of 700-1060 mL/min. It was observed that the pH stabilized at about 5.6. This was consistent with values predicted by OLI steam Analyzer for water equilibrating with carbon-dioxide in ambient air. When compared with experiments from the earlier work the systems studied in these sets of experiments equilibrated at a higher pH value as can be seen in Figure 11. This could be due to bubble interference in pH measurements, calibration errors or other artifacts that could have affected the earlier experiments discussed in Chapter 1. It was also observed that when controls were run side by side with DI water aerated through HFM, the aeration process increased the kinetics of equilibration with atmospheric CO_2, as can be seen in Figure 12. This would mean that the model solutions used to simulate supersaturation would have to be

equilibrated with the atmosphere before running experiments. It was evident from these experiments that the dynamics of pH equilibration of CO_2 with the aqueous phase is a consideration that cannot be ignored whilst using pH as a metric to measure the kinetics of the crystallization process. Moreover, this may assume increased significance when the system is subjected to aeration to study the effects of bubbles possibly acting as nucleation sites.

Besides pH measurements, conductivity was also measured. The conductivity of the aerated system and control hovered in the range of about 1 μS/cm. This closely matches with the equilibrium predictions made by OLI stream analyzer. The use of changing conductivity to track kinetics may not be significantly impacted because the change sensed due to aeration is in the order of 1 μS/cm, the conductivity of supersaturated solutions used are in the order of 5-6 mS/cm.

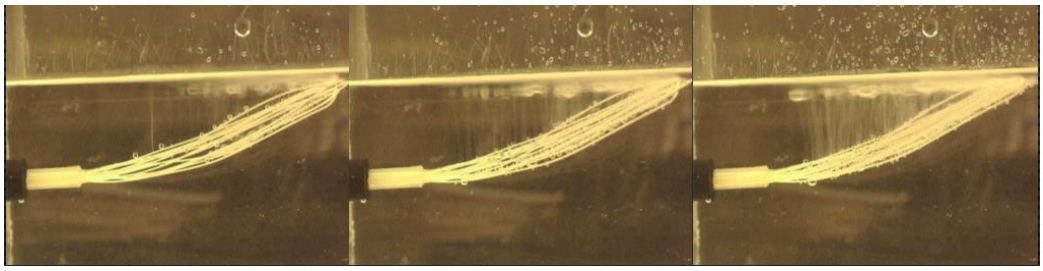

Bubble contact with 1L solution, the air flow rate has been increased from left to right for better image capture.

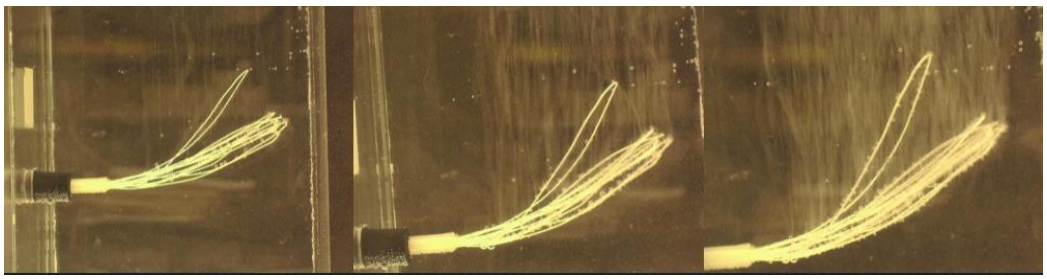

Bubble contact with 2L solution, the air flow rate has been increased from left to right for better image capture.

Figure 10- Comparison of bubble contact for 1L and 2L jars.

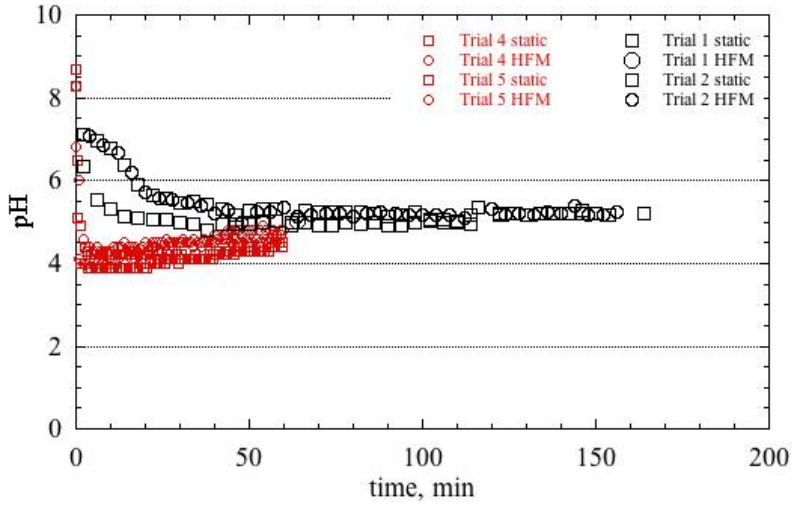

Figure 11- Comparison of pH values at equilibration when DI water is aerated with HFM.

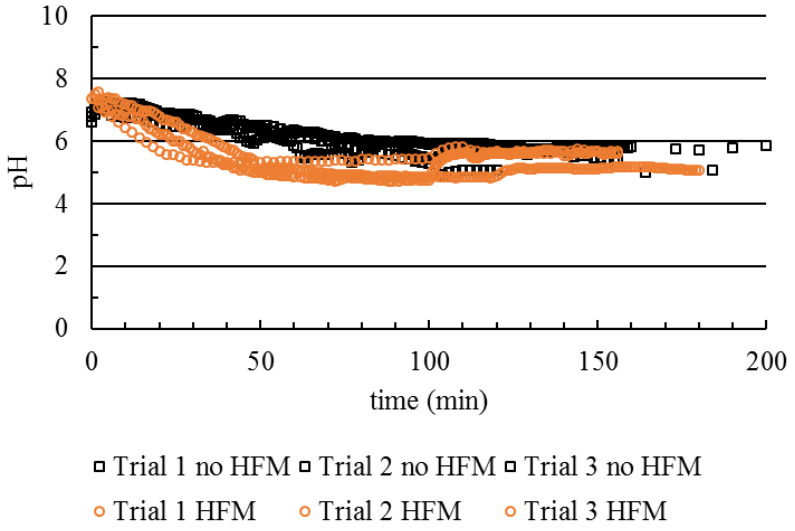

Figure 12- Comparison of DI water equilibration with CO_2 for static and HFM aeration trial.

3.3 Effect of silica on crystallization

As previously mentioned in Chapter 1, the solution 2 of the crystallizing electrolyte system included a small amount of silica. The silica particulates were largely insoluble in the aqueous phase in the timescale of our mixing. Thus, in theory these undissolved small silica particulates can act as nucleation sites, thereby interfering with the induction phase of crystallization or, for that matter, the entire process of crystallization kinetics. Thus, experiments were carried out in

batch mode using the solution 2 with and without silica. Further the effect of HFM aeration and the influence of in-situ and grab sampling of pH and conductivity measurements were also studied. The plots of pH, conductivity and turbidity vs. reaction time without any aeration or stirring is shown in Figure 13.

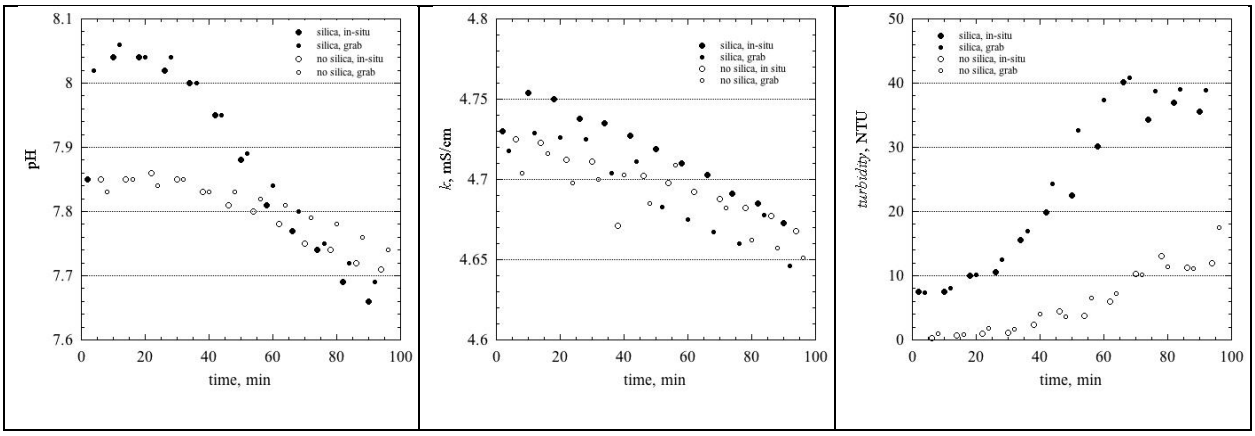

Figure 13- pH, conductivity and turbidity versus time for batch experiments without aeration or stirring (grab and in-situ sampling for pH and conductivity).

From Figure 13 it can be observed that when a small amount of silica particles are added to the crystallizing solution, significant change in turbidity and pH trends can be observed. It is also important to note that significant differences cannot be observed between grab and in-situ sampling techniques. Whilst, this may be the case, when the same experiments were performed under the influence of HFM aeration it was observed that significant difference in pH, conductivity, and turbidity slopes between the presence of silica and absence of silica was not observed. However, the overall values of pH, conductivity, and turbidity were different from the trials conducted in the absence of aeration. This may be due to the highly sensitive nature of the measurement techniques to minor differences in electrolyte concentration and varying levels of equilibration of crystallizing liquor in terms of CO_2 concentration with the ambient. The plots of pH, conductivity and turbidity versus time for aeration experiments with and without silica are shown in Figure 14. Again, experiments were performed using both grab and in-situ sampling for pH and conductivity.

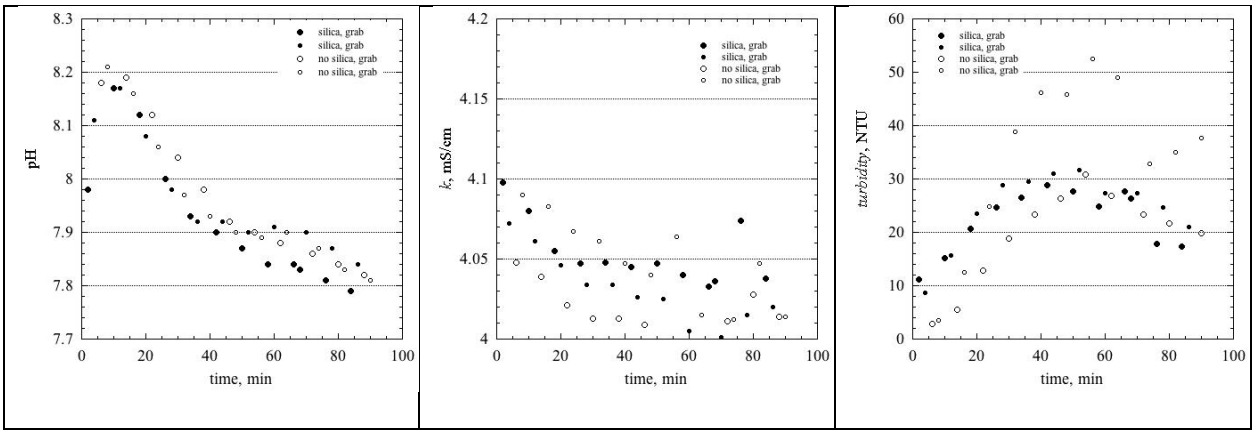

Figure 14- pH, conductivity and turbidity versus reaction time plots for aerated trials, with and without silica (grab and in-situ sampling for pH and conductivity).

The next set of experiments were performed to study crystallization kinetics in side-by-side trials in which the only variation is whether there is a stagnant system (no aeration or stirring), aeration by means of air bubbling and using the hollow fiber membrane aeration device, silica not present in all three trails. Only turbidity measurements show some evidence of aeration impacting crystallization kinetics. This may not necessarily be indicative of aeration significantly affecting crystallization kinetics as increased turbidity could just be indicative of better mixing that allows for more solids to be in suspension as opposed to settling when compared to stagnant trials. The plots are shown in Figure 15.

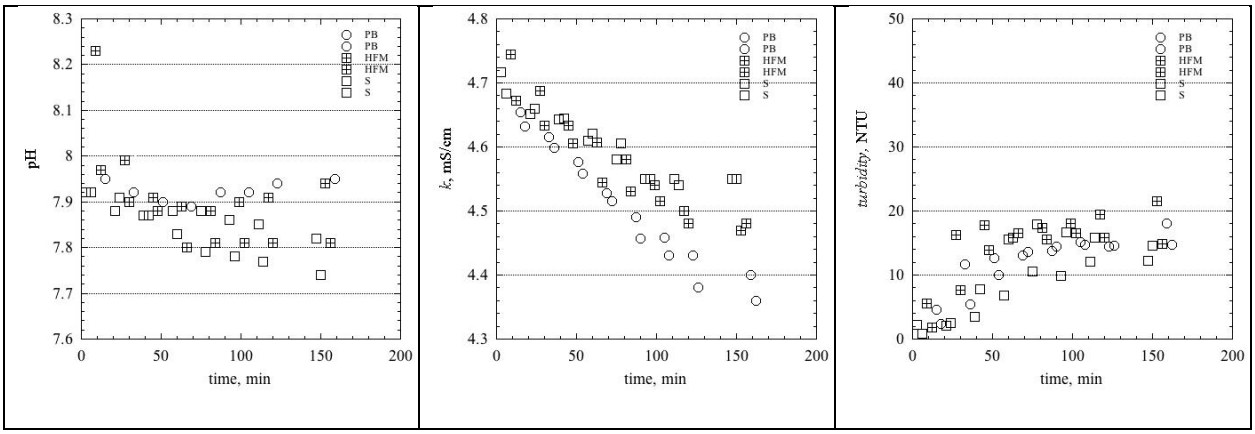

Figure 15- Batch crystallization with two replicates each aeration for no stirring, aka stagnant (S), aeration from a plain tube bubbling without additional stirring (PB), aeration using HFM aeration device without additional stirring. (No silica, turbidity is always measured by grab sampling).

3.4 Equilibration of solutions with CO_2

The binary electrolyte system that comprises the crystallizing solution incorporates $NaHCO_3$ salt (solution 2).

$$NaHCO_3 + H_2O\ (DI) \rightarrow Na^+ + H_2CO_3 \rightleftarrows HCO_3^- + H^+ \rightleftarrows CO_3^{2-} + 2H^+ \quad (1)$$

$$CO_2(g) + H_2O\ (DI) \rightarrow CO_2(aq) \rightarrow H_2CO_3 \quad (2)$$

Equation 1 represents the ionization of sodium bicarbonate ($NaHCO_3$) and the equilibrium of carbonate and bicarbonate species in solution.

The DI water used to prepare solutions is devoid of CO_2 at the outlet of the treatment system, as soon as it is in contact with the ambient, it starts equilibrating with CO_2 in the atmosphere as represented in equation (2). As more aqueous CO_2 dissolves in solution, though the equilibrium between carbonate species is the same, the total concentration of carbonate species increases. The equilibration of DI water with atmospheric CO_2 has a kinetics associated with it. Thus, if the prepared solution 2 is not adequately in equilibrium with atmospheric CO_2 though the equilibrium of the carbonate speciation will remain unchanged, this would have an effect on the total

concentration of carbonates in the solution. The total concentration of the carbonates has a bearing on the equilibrium precipitation of $CaCO_3$. This factor was not found to be significant as little or no conductivity increases were observed in DI water control experiment, as discussed previously. If CO_2 absorption significantly changed the carbonate concentration, more significant conductivity changes should have been observed in DI water equilibration tests. Nonetheless, the potential effect on the material balance, due to the addition of CO_2 into solution, from atmospheric equilibration, needs to be accounted for as well. As can be observed from equation (3) the precipitation of $CaCO_3$ involves the release of CO_2.

$$CaCl_2 + MgSO_4.7H_2O + Na_2SO_4 + NaHCO_3 + SiO_2 + H_2O \rightarrow$$

$$Ca^{2+} + 2Cl^{-1} + Mg^{2+} + SO_4^{2-} + Na^{+} + HCO_3^{-} + CO_3^{2-} + SiO_2\,(s) + CaCO_3(s) + CaHCO_3 +$$

$$NaHCO_3 + Mg(HCO_3)_2 + CO_2 \uparrow \qquad (3)$$

Chapter 4

4.1 Steady state crystallization analysis

Besides the qualitative understanding of crystallization mechanisms, it is important to quantify the kinetics and we are using $CaCO_3$ crystallization as a model system to evolve a measurement and analysis framework. The improved understanding of crystallization kinetics is necessitated by the need to improve membrane processes such as reverse osmosis (RO). It is interesting to note that most previous studies pertaining to the study of crystallization have involved studying supersaturated electrolyte systems in batch reactor modes [1-4]. In the present study, we have approached the kinetic analysis of $CaCO_3$ system using a steady state framework as opposed to the more frequently-used unsteady-state batch systems.

Previous researchers have discussed mixed-suspension-mixed-product-removal (MSMPR) crystallizer [15-19]. An MSMPR crystallizer is based on a steady state principle and the degree of supersaturation is determined by the residence time of the crystallizing solution in the crystallizer [15]. $CaCO_3$ crystallization has been previously studied in such an MSMPR system using a population balance model wherein a mathematical model was developed to study the increase in crystal size in an MSMPR crystallizer in relation to the number density of crystals [18]. A staged MSMPR system with solids recycle to study kinetics has been reported as well, the method used incorporated a stage system of MSMPRs where the exit stream of the last MSPR in the system was recycled back into the inlet stream to the first MSPR of the setup. By using this approach the researchers demonstrated a seeding process through recycling, where the seed particulates were crystals themselves as opposed to foreign particulates [21]. In the present study, a CSTR-in-series system has been used to study the kinetics of crystallization exclusively. Though we have used turbidity as the key metric to quantify crystallization we have not approached kinetics using a

population balance model. We have used precipitate collection and analysis of supernatant ion concentrations to quantify crystallization as opposed to a population balance approach.

4.2 Ideal continuously stirred tank reactor (CSTR)

A CSTR is an ideal chemical reaction engineering concept. It is a continuous flow reactor of volume V, where feed enters the reactor continually at a flow rate v_o and therefore is retained for a specified average residence (or retention) time. The residence time τ is given by V/v_o. Successive CSTRs-in-series can be arranged in such a way that the second reactor processes the outlet of the first reactor as feed, the third processes that of the second and so on. A system of infinite CSTRs-in-series corresponds to a plug flow reactor, another reaction engineering idealization [20]. In the case of an ideal CSTR, the reactor is assumed to be well mixed and without concentration gradients in the bulk; concentration of the bulk is assumed to be the same as that of the outlet stream of the CSTR. Nonetheless, a CSTR operation involves an unsteady state process at startup, i.e., when the CSTR is first filled up by the feed to a volume V and thereafter till a concentration profile that does not vary with time. In our case, after a steady concentration is reached in the bulk of all CSTRs in the series setup, the CSTR-in-series system is said to be operating at steady state [20]. An MSMPR crystallizer is a CSTR that is specifically used for crystallization [21].

The concept of using CSTRs-in-series enables the isolation of the composition of the electrolyte system corresponding to various timescales. In the case of multiple CSTRs operating in series the level of supersaturation in each CSTR is a function of the overall sum of residence times, or overall reaction time [20]. The process of using CSTRs operating in series at steady state would allow estimation of equilibrium crystal yield at a given level of supersaturation. In the case of a batch system, the analysis of the kinetics of a supersaturated system that exhibits crystallization phenomena can be conducted only in an unsteady mode. There are certain advantages to the steady

state analysis as opposed to an unsteady state monitoring in terms of understanding the kinetics that governs the said system—primarily, the sampling (analysis) in an unsteady system is difficult to get precise, while the composition (and state-of-the-system) in each CSTR is mostly unchanging (in the ideal sense) for a specific CSTR and the time constant it represents.

By modifying the retention time of fluid elements in CSTRs-in-series, the electrolyte system at a certain nucleation stage (or pre-nucleation stage) can be isolated within an individual CSTR. Thus, the induction time of nucleation can be better approximated using the CSTRs-in-series configuration. In the case of steady state analysis, data such as pH, conductivity and turbidity can be acquired in replicates across the CSTRs for the overall extent of crystallization each one represents. Therefore, data can be acquired within a statistical band and would thus be more reliable. Also, interestingly, the statistical bandwidth of the data acquired using steady state monitoring of the crystallization phenomena could provide an insight into the extent of the variance of process parameters of what is essentially a stochastic process. In our experiments reaction time is defined as the time the crystallizing liquor has spent in the overall CSTRs-in-series setup.

It is hoped that this method of CSTRs-in-series helps to identify if a particular process intervention applied at a particular reaction time can be used to reduce the induction time i.e. induce crystallization earlier. Therefore, the steady state system can be used to collect kinetic data more accurately, better approximate induction time and help evaluate process changes that could improve crystallization kinetics. The approach discussed in this chapter, leans towards an approach that makes use of conductivity, pH, and turbidity measurements to track the kinetics of the process as opposed to a population number model or a crystal size growth based kinetic measurement. These latter techniques are more instrument intensive and less useful for early process scoping. To

evaluate methodologies that can be applied to enhance crystallization, initially a robust method to measure the kinetics of crystallization is a prerequisite.

4.3 Steady state and startup of reactors (aka crystallizers)

In the case of steady state operations, it is important to deduce when the system reaches steady state after initial startup. The time between reactor startup and steady state is termed as stabilization time. In our experiments, reliable estimation of stabilization time is required so that kinetic parameters can be measured at steady state operation. We empirically considered the kinetics to be a first order reaction and considered the CSTRs to be ideal. Stabilization time (t_s) is given by. $t_s=4.6\tau/ (1+ \tau k)$, where k is the first order rate constant. For very slow reaction rate constants, $t_s \sim 4.6\tau$. For fast reactions $t_s \sim 4.6/k$. In the case of most first order reactions stabilization is achieved within three to four residence times [20].

$$\lim_{k\to 0} \frac{4.6\tau}{1+\tau k} = 4.6\tau$$

Thus t_s, even for the slowest of reactions should not exceed 4.6τ.

4.4 Results and discussion

4.4.1 Residence time distribution experiments

Residence time distribution (RTD) were conducted as described in section 2.3.5. Figure 16b shows the measured exit age distribution curves E(t) for two τ values 5.2 and 2.4 min for each of 1 through 6 CSTRs-in-series. The exit age distribution (E(t)) is given by $E(t) = \frac{C(t)}{\int_0^\infty C(t)dt}$, where C(t) is the function of concentration of tracer with respect to time (t). The cumulative mean residence time (t_m) is given by $t_m = \int_0^\infty tE(t)dt$. The variance ($\sigma^2$) is given by $\sigma^2 = \int_0^\infty (t-t_m)^2 E(t)dt$. Standard deviation (σ) is the square root of variance [20].

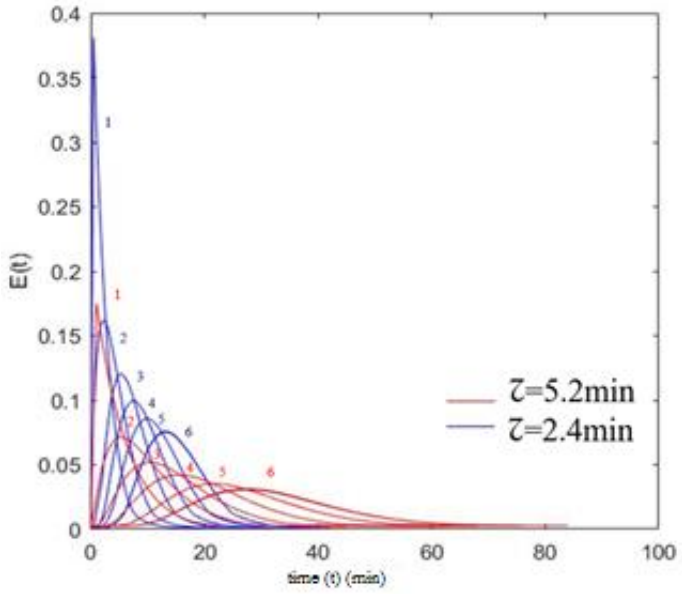

Figure 16- Residence time distribution (RTD) for $\tau = 2.4$ and $\tau = 5.2$ min.

The changing shape of the E(t) curves can be observed for both τ values. In an ideal scenario, the pulse input and the pulse response are perfect normal distributions with skewness (s_1) = 0. Skewness (s_1) is defined as thus [24]

$$s_1 = \frac{\left(\frac{1}{n}\sum_{i=1}^{n}(x_i - \bar{x})^3\right)}{\left(\sqrt{\frac{1}{n}\sum_{i=1}^{n}(x_i - \bar{x})^2}\right)^3}$$

Where n is the number of elements in the population x_i (in this case E(t)) is an individual element of the population, $\bar{x}$ is the mean. We made use of the bias corrected skewness (s_0) that corrects for errors due to population size.

$$s_0 = \frac{\sqrt{n(n-1)}}{n-2} s_1$$

Table 4 lists the skewness for $\tau = 5.2$ and 2.4 min.

Table 4- Bias corrected skewness of E(t) curves, cumulative mean residence time and variance of distribution for $\tau \sim 2.4$ and $\tau \sim 5.2$ min.

#tanks in series	bias corrected skewness (s_0)		cumulative mean residence time (t_m) (min)		standard deviation (σ) (min)	
	$\tau \sim 2.4$ min	$\tau \sim 5.2$ min	$\tau \sim 2.4$ min	$\tau \sim 5.2$ min	$\tau \sim 2.4$ min	$\tau \sim 5.2$ min
1	2.40	1.46	2.57	5.37	3.72	4.42
2	1.07	0.96	4.43	10.81	7.12	7.97
3	0.85	1.01	7.35	16.94	10.33	11.36
4	0.81	0.82	9.61	22.10	13.28	12.50
5	0.78	0.76	12.02	28.39	17.15	14.21
6	0.61	0.60	15.20	33.33	18.96	14.57

It can be observed that the s_0 values are high for fewer tanks in series than in the case of six tanks in series. As the number of tanks tends to infinity the s_0 will converge to 0. It can be observed from Figure 16 that as the number of tanks increase the dispersion of tracer increases. Table 4, in the case of $\tau \sim 2.4$ minutes, σ values are greater than t_m values. In the case of $\tau \sim 5.2$ minutes, σ values are closer to the corresponding t_m values and σ exceeds t_m only in tanks 2 and 3.

This could point to a situation wherein the impeller rotational speed of 45 rpm (which was arbitrarily chosen for initial experiments so as to minimize splashing and tangling when including the HFM aeration) was not sufficient to maintain the individual tanks in the CSTRs-in-series set up well-mixed for lower τ values i.e. higher flow rates (v_o).

4.4.2 Induction time for crystallization

The induction phase as discussed in earlier chapters pertains to the time lag between achieving supersaturation and the appearance of discernible crystals. We have chosen a value of 5 NTU to define the first appearance of crystals in our experiments. It is also important to note that crystals

were not visually observable in the liquor at turbidity values less than 5 NTU. Experiments were performed to test this hypothesis using six tanks in series with 1L volume.

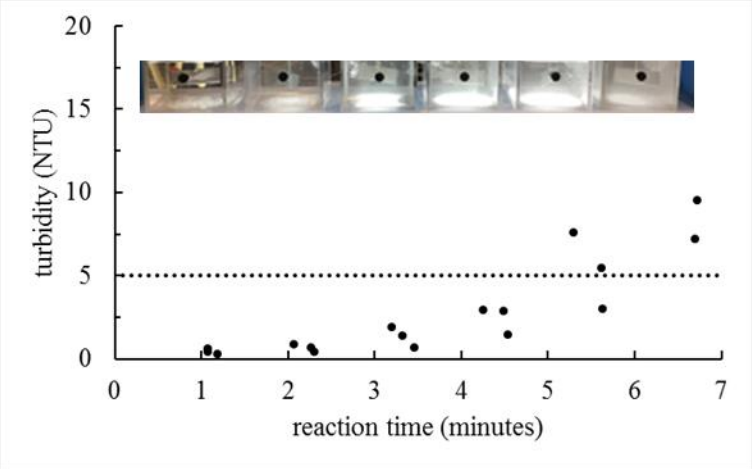

Figure 17- Turbidity vs. reaction time. Six tanks in series each with residence time 1 min. (3 trials. The dotted line is the 5 NTU mark. An image of a reactor system where turbidity in 6th tank >5 NTU is also shown (its volume was 2L).

It can be observed from Figure 17 that turbidity becomes visually discernible only for cases where turbidity exceeds 5 NTU. There the key metric that was used to measure the progress of crystallization kinetics is turbidity.

4.4.3 CSTRs-in-series crystallization experiments

Primarily the experiments involved running six CSTRs-in-series such that the average residence time (τ) in each CSTR was ~5±0.4, ~2.2±0.2, and ~11±0.5 min. The residence time of the liquor in the connecting tubing between tanks was also taken into account, this adjustment to the overall all residence time would not impact the first tank in the setup. The residence time in the tubing was about 0.002 min for τ~2 min, 0.168 min for τ~5 min, 0.371 min for τ~11 min. It was observed that the turbidity values consistently increased across reactors for all experiments. It was also important to note that the measurements of pH and conductivity did not tend to reflect much change

in the system, as was observed in batch experiments discussed in chapters 1 and 2. Thus, the main kinetics-related metric for CSTRs-in-series experiments was turbidity.

Turbidity is the measure of suspended solids in a liquid medium. The factors that affect turbidity measurements include the number density of particulates, optical characteristics, size, and morphology of particulates (refer to appendix A for more details on turbidity). Though turbidity may not theoretically have the same level of confidence when compared to metrics such as conductivity or pH, in the present experiment the measure of turbidity proved to be a consistent method to track the kinetics of the system.

Figure 18(a) shows turbidity (NTU) versus overall reaction (crystallization) time (min) for $\tau \sim 2.2\pm0.2$, 5 ± 0.4 and 11 ± 0.5 minutes. Figure 18(b) shows turbidity (NTU) versus normalized time or the #tank. It can be clearly observed that the rate of crystallization (initial slope) appears to be higher for lower τ values. The normalized plot Figure 18(b) also shows the differing rate of crystallization for various τ values. Thus, besides overall reaction time, certain other factors appear to influence the crystallization process. These factors will be discussed in detail in the following sections.

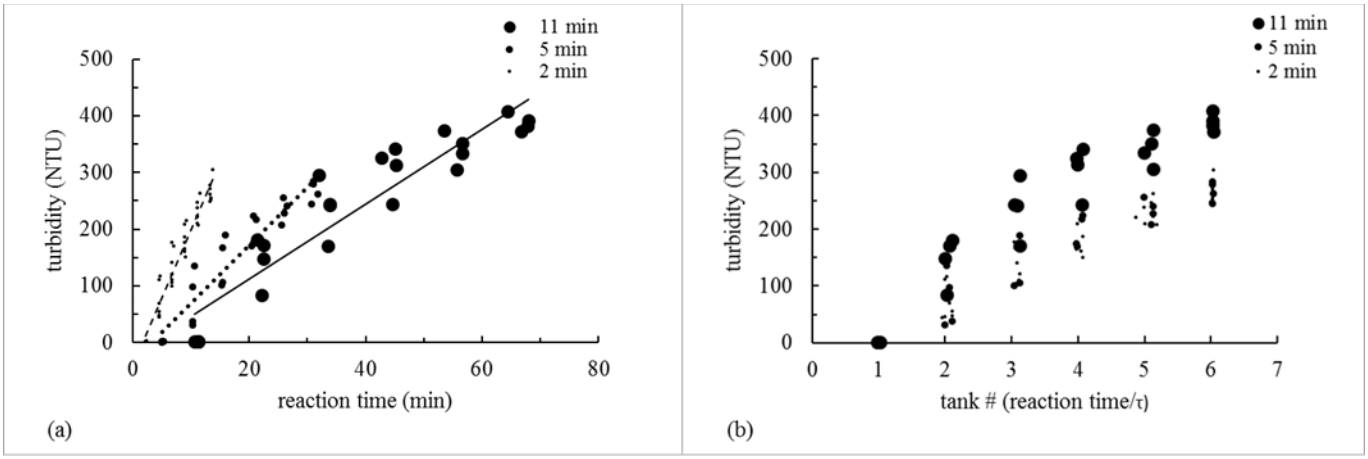

Figure 18-(a) turbidity (NTU) vs. reaction time (min). (b) turbidity (NTU) vs. tank # (reaction time (min)/τ).

pH readings were also measured at steady state. The pH for all cases shows a declining trend. But then except for $\tau \sim 2$ min experiments the pH shows a wide divergence between replicates and provides no reproducible information on induction time, Figure 19. The decline is pH in the reaction time and normalized time plots are due to a decrease in alkalinity as CO_3^{2-} ions are precipitated as carbonate.

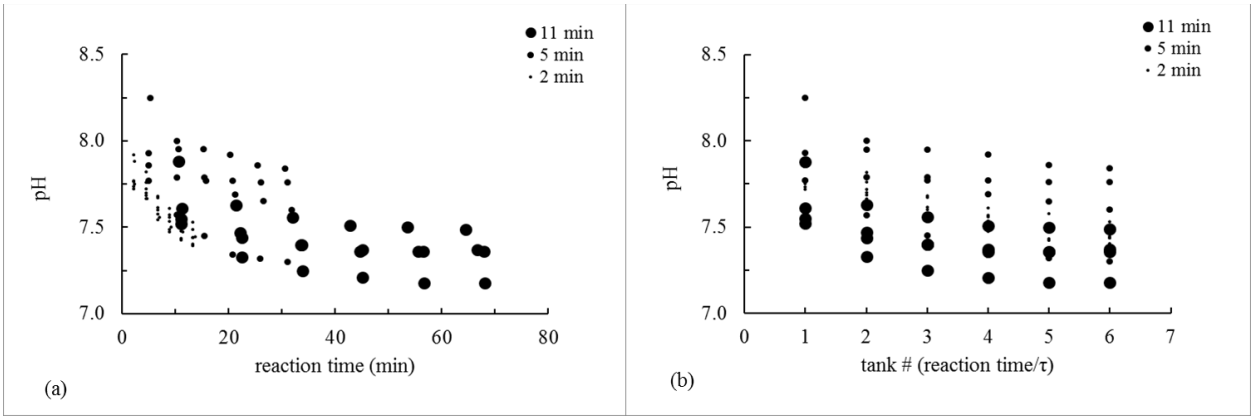

Figure 19- (a) pH vs. reaction time (min). (b) pH vs. tank # (reaction time (min)/τ).

Whilst there is a possibility that turbidity changes could be solely due to changes in particle morphology and/or number density whilst the mass of crystals remains constant. The declining pH suggests that the change in turbidity indicates increased precipitation.

4.4.4 Post-crystallization analysis of CSTRs

After performing the crystallization reactions, the contents of the CSTRs were emptied out and allowed to dry. It was observed that in the case of the six CSTRs-in-series setup the reactors showed a decreased level of scaling from the 2nd to the 6th CSTR. The 1st CSTR in which no visible crystallization was observed showed little to no scaling and in the case of the 6th CSTR very little scaling was observed on the walls of the CSTR. A possible explanation could be that the time the supersaturated solution spends in the 1st CSTR could point to the induction time. As the saturated solution reaches the second tank, and after the induction phase time lag, the high level of supersaturation prefers a heterogeneous nucleation pathway wherein the walls of the CSTRs act

as sites. As the liquor moves to successive CSTRs the supersaturation is lowered and the preferred pathway could be homogeneous nucleation. Figure 20 shows the scaling across tanks (1-6) for different τ values.

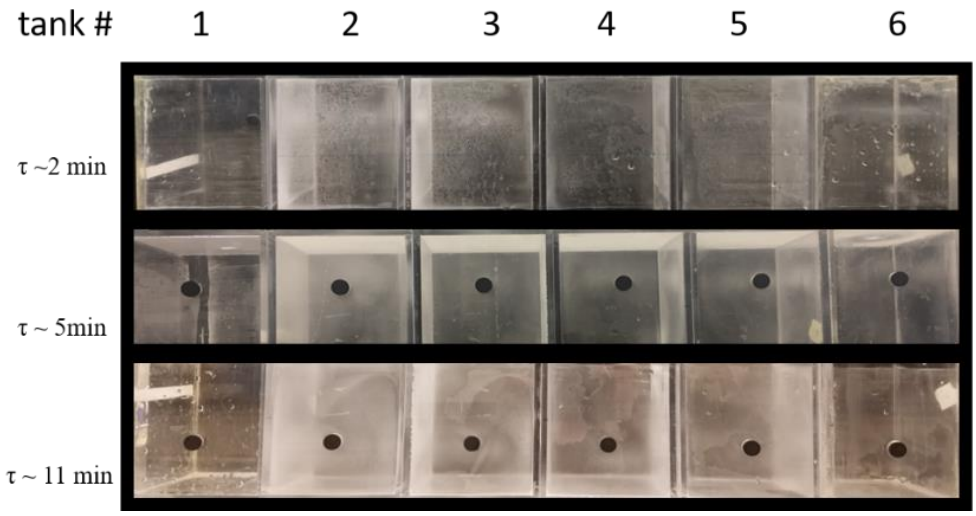

Figure 20- Scaling on the empty acrylic tanks after a crystallization experiment. Observe that for all τ values there is very little scaling in the first and sixth tank but excessive scaling in the second one followed by decreasing scaling until the sixth.

4.4.5 Effect of surface area and residence time.

Experiments were performed with several nominal residence times, as previously mentioned. It is reasonable to expect more total crystallization with longer overall reaction times, i.e. residence times. Interestingly, since crystallization is a surface dependent phenomena, thus, besides residence time, the surface area of each reactor (A_T) exposed may also be an important factor. It can be observed from Table 5 that the A_T/v_o is higher in the case of lower τ values i.e. higher flow rates. Besides the actual reaction time that the crystallizing solution spends in the reactor system this aspect has the potential to influence crystallization kinetics with respect to the influence of heterogeneous crystallization discussed in chapter 1. The walls of the reactors would act as nucleation sites, thereby increasing the rate of crystallization.

Table 5- A_T/v_o values for $\tau \sim 2$, 5, and 11 min

nominal residence time (τ), each tank (min)	**volumetric flow rate (v_o) (m^3/s) x10^6 for reactor volume 1.75 x 10^{-3} m^3**	**A_T/v_o (s/m) x 10^4**
2	14.6	0.49
5	5.83	1.23
11	2.65	2.72

area of 1 CSTR (A_T) ~720 cm^2

4.4.6 Effect of mixing (impeller action)

Each tank is equipped with a stirrer rotating at an average rate of 45 rpm. Since crystallization can also be impacted by mixing, or the impeller speed, we have proceeded to characterize the effect of the impeller in terms of the nondimensional impeller Reynolds number (Re_{Im}).

The equation of impeller Reynolds number (Re_{Im}) is given by [25]

$$\frac{N_{Im} D_{Im}^2 \rho}{\mu}$$

To estimate the power associated with agitation by the impeller we estimated the value of Newton number (N_p) using the empirical formulations developed by Furukawa et al [26]. The power associated with the impeller (P_{Im}) is given by the expression [26]:

$$P_{Im} = N_p \rho N^3 D_{Im}^5.$$

Where, ρ is the density of the liquid (water), N is stirrer rotation speed in s^{-1}, D_{Im} is the diameter of the impeller. The energy dissipation (ε_{Im}) of the impeller can be calculated by P_{Im}/M_{CSTR} (M_{CSTR} is the mass of solution in one CSTR). The values used to derive Re_{Im} and P_{Im} are shown in Table 6.

Table 6- Parameters for calculating ReIm, PIm, ε, η values for impeller.

parameter	**value**	**units**
N_{Im}	0.75	s^{-1}
diameter of blade (D_{Im})	0.076	m
density of water (ρ)	1000	kg/m^3
viscosity of water (μ)	1.002×10^{-3}	$N \cdot s/m^2$
Newton number (N_p)	0.26	-
mass of liquid in each CSTR (M_{CSTR})	1.75	kg
kinematic viscosity of water (ν)	1.004×10^{-6}	m^2/s

Using parameters listed in Table 6, we get $Re_{Im} = 4.32 \times 10^3$. Reynolds number is a commonly used dimensionless number that can be used for scaling designs and provides an idea on the scale of turbulence i.e. mixing. It can be observed in our case that the Reynolds number is in the order of 10^3 indicating that the mixing may not be thorough and this correlates with the dispersion in tracer studies discussed in section 4.4.1. The power associated the impeller (P_{Im}) was calculated to be 2.78×10^{-4} $kg \cdot m^2 \cdot s^{-3}$. ε_{Im} was calculated to be 1.59×10^{-4} $m^2 \cdot s^{-3}$. The calculated values are shown in Table 7.

Table 7- Calculated impeller mixing attributes.

parameters	value
Reynold number (Re_{Im})	4.32×10^{3}
power (P_{Im}) ($kg \cdot m^2 \cdot s^{-3}$)	2.78×10^{-4}
energy dissipation(ε_{Im}) ($m^2 \cdot s^{-3}$)	1.59×10^{-4}

4.4.7 Effect of mixing (peristaltic pumping)

It was interesting to observe that for experiments conducted with different τ values, crystals appeared in the second tank of the six-tank reactor system irrespective of the τ value. This would mean that for a $\tau \sim 2$ min reactor system extensive turbidity and crystallization is observed at reaction times equivalent to ~4 min whereas in the case of $\tau \sim 11$ min experiments' turbidity and visual appearance of crystals was observed only at reaction times equivalent to ~22 min, etc. Besides the effects discussed in sections 4.4.5 and 4.4.6, the peristaltic pumping effect on solution mixing between tanks also appears to have a significant effect on crystallization.

We hypothesize that the peristaltic pumping action affects a certain level of mixing within the pump tubing that allows for enhanced nucleation within the tubing. It is also interesting to observe that the Re calculated for τ values in consideration indicated a laminar flow regime. Moreover, the peristaltic pumps were driven at a higher rpm than required (100% higher) in order to be sure to maintain requisite volumes in CSTRs using this dynamic weir system. It was visible through the transparent tubing that the liquid was transported as slugs and not as a continuous train of fluid for the most part. Moreover, the impinging of rollers on the tubing deforms the tubing resulting in a constriction of flow. The complex fluid dynamics involved in the peristaltic pumping cannot be characterized easily. We nevertheless have attempted to analyze the flow metrics assuming fully developed flow in the tubing which is not the case. Considering the pumping tube to be a pipe of

length 0.12 m (average length of tubing between CSTRs), we calculated the total pressure drop in the tubing using the Darcy-Weisbach equation [27].

$$\frac{\Delta p}{L} = \frac{\rho}{2} f_D \frac{u_{avg}^2}{D}$$

Δp can be calculated by knowing the length of the tubing (L) the density (ρ), velocity of flow in tubing (u_{avg}), diameter of the tube (D) and Darcy friction factor f_D can be calculated by the empirical relationship between the friction factor (f_D) and Reynolds number (Re) [27].

$$f_D = \frac{64}{Re}$$

The pressure drop represents the losses due to friction in the tubing. With pressure and volumetric flow rate entering the tubing we obtained the power associated with the fluid transport. The ratio of power and the volume of fluid present in the tubing provides the energy dissipation (ε). Power (P_{tube}) is obtained by considering the pressure drop as the working pressure of the fluid (Δp) in transport and the volumetric tube flow rate (q).

$$P_{tube} = \Delta p \text{ x } q$$

The energy dissipation (ε_{tube}) can then be calculated from the power (P) and the control volume (V_c) and density of fluid (ρ), V_c is same as q considering unit time. The energy thus dissipated is indicative of the intensity of pumping action. The energy dissipation can be used as a measure to gauge the extent of mixing imparted to the fluid in transport. In the first tank the crystallizing liquid is pumped in as a separate system of two different electrolyte solution (solution 1 and solution 2), so this pump-based mixing is not relevant in it.

It can be observed from Figure 21 that there is no peristaltic stage for liquid coming into the first tank but every tank other than the first tank has a peristaltic stage preceding the tank.

$$\varepsilon_{tube} = \frac{P_{tube}}{\rho V_c}$$

Table 8- Energy dissipation for τ = 2, 5 ,11 min

residence time (τ) (min)	tube flow rate (q) $x10^6$ (m^3/s)	u_{avg} $x10^1$ (m/s)	Re $x10^{-2}$	f_D $x10^2$	$\Delta p/L$ $x10^{-1}$	p $x10^{-1}$ (Pa)	power (P) $x10^5$ ($kg \cdot m^2 \cdot s^{-3}$)	energy dissipation $x10^2$ ($m^2 \cdot s^{-3}$)	
								ε_{tube}	ε_{Im}
2	14.6	2.98	23.5	2.73	15.3	18.4	268	18.4	0.016
5	5.83	1.19	9.39	6.82	6.12	7.34	42.8	7.34	0.016
11	2.65	0.54	4.27	15	2.78	3.34	8.85	3.34	0.016

Table 8 provides the values of tube flow energy dissipation thus calculated for different residence times (τ). It can be observed that for a given level of supersaturation the energy dissipation for higher flowrates i.e. lower τ values the energy dissipation is higher.

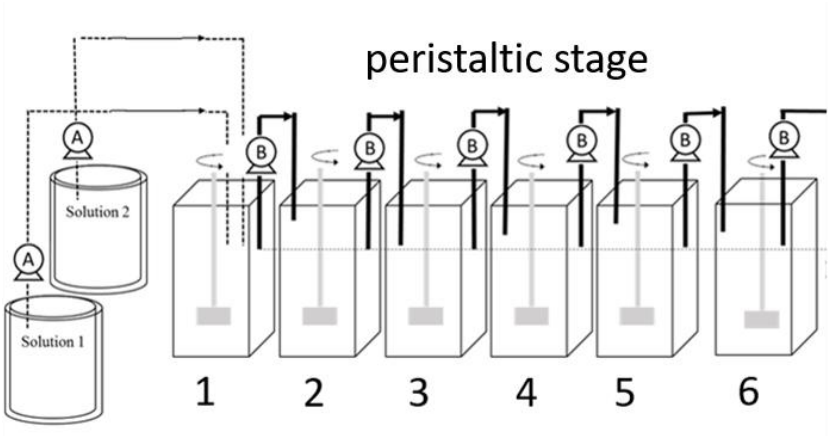

Figure 21- Observe that there is no peristaltic stage for liquid coming into the first tank but every tank other than the first tank has a peristaltic stage preceding the tank.

Thus, the net dissipation in the first tank would only be due to the impeller action while in successive tanks dissipation is due to the impeller and peristaltic pumping.

$$\varepsilon_{tot} = \varepsilon_{Im} + \varepsilon_{tube}$$

ε_{Im} is the same in all tanks across all τ values (the rotation speed for all experiments was ~45 rpm. ε_{tube} is the same for all stages for a particular τ value. It is also interesting to note that ε_{tube} values are 2-3 orders of magnitude above that of ε_{Im}, thus the peristaltic mixing seems to impact crystallization more than the impeller action. The Kolmogorov mixing theory envisages that the

macroscale eddies cause mixing through constant energy dissipation resulting in smaller and smaller eddies which then ultimately reach a very small scale where turbulence is universal i.e. at the Kolmogorov scale all eddies have the same characteristics. This universal scale can be estimated using dimensional analysis. Kolmogorov scales depend only on dissipation and viscosity of process fluid. The Kolmogorov mixing scales (η_2, η_5, η_{11}) for the τ values 2, 5, and 11 min were calculated. The mixing scale associated with Kolmogorov mixing length was calculated by the expression [28].

$$\eta = \left(\frac{\nu^3}{\varepsilon_{tot}}\right)^{1/4}$$

The mass transfer Fourier number (F_o) gives the ratio of macro scale transport to diffusive transport. Ruzicka et al. define F_o as the ratio of unsteadiness and turbulent mass diffusion [29].

$$F_o = \frac{\eta^2}{D_a t_c}$$

Here D_a is diffusivity, t_c is characteristic time and η refers to the mixing scale length. For all cases, we have taken D_a to be the diffusivity of Ca^{2+} ions in sea water at 23 ^{0}C (9.8 x 10^{-6} cm^2/s) [30]. At small mixing scale lengths and high power input relative to the size of vessels molecular mixing is almost simultaneous, thus $F_o \sim 1$. Moreover, the assumption Fo ~ 1 allows estimating a time scale at which the mass transfer will be significant enough that diffusion through the estimated Kolmogorov length scale is not the rate limiting mass transfer coefficient. The total dissipation (ε_{tot}) was calculated from the contributions from peristaltic and impeller action (ε_{tube} and ε_{Im}). Damkohler number of the second type (Da_{II}) is defined as the ratio of chemical reaction rate to the molecular diffusion rate. Considering that reaction rates are not within the scope of this study, we approximated the chemical reaction rate parameter as residence time and t_c values were chosen to be the parameter to describe molecular diffusivity.

Table 9- Length scales and characteristic times for different τ values in a 6 CSTR in series setup

residence time	**parameters**	**1st tank**	**2nd-6th tank**
tank 1 2 min (τ_2) tank 2-6 2.002 min	dissipation (ε_{tot}) (m^2s^{-3}) x 10^4	1.59	1836.83
	length scale (η_2) (m) x 10^5	28.24	4.84
	characteristic time (t_c) (s)	81.43	2.40
	Damkohler no. II type (Da_{II})	1.47	50.05
tank 1 5 min (τ_5) tank 2-6 5.168 min	dissipation (ε_{tot}) (m^2s^{-3}) x 10^4	1.59	735.68
	length scale (η_5) (m) x 10^5	28.24	6.09
	characteristic time (t_c) (s)	81.43	3.78
	Damkohler no. II type (Da_{II})	3.68	82.03
tank 1 11 min (τ_{11}) tank 2-6 11.37 min	dissipation (ε_{tot}) (m^2s^{-3})	1.59	335.27
	length scale (η_{11}) (m) x 10^{-5}	28.59	7.41
	characteristic time (t_c) (s)	81.43	5.60
	Damkohler no. II type (Da_{II})	8.1	121.82

It can be observed from Table 9 that the characteristic time scale (t_c) values are lower in the case of lower τ values. This points to a higher level of mixing intensity in the case of reactor operations where the residence time spent by the crystallizing solution is lower than when compared to higher residence times. This is explainable by the fact that the peristaltic action is a significant source of mixing and in the case of τ = 2 min the crystallizing liquor is subjected to a peristaltic stage every 2 minutes. In the case of τ = 5 and 11 min the liquor is subjected to peristaltic pumping every 5

and 11 min, respectively. The estimated values of Da_{II} suggest that for the slow reaction in tanks mass transfer limitations do not appear to be significant for the slow rates of precipitation observed. The approximation of reaction rate in terms of residence times may not be accurate. Further studies are required to understand the mass transfer characteristics of the process.

4.4.8 Precipitate collection and analysis of supernatant

Experiments were conducted to collect the precipitate from the 6th tank for experiments with τ = 2.2±0.2, 5±0.4, and 11±0.5 min. As described in section 2.3.4 the precipitate was collected, weighed and the permeate was sent for ICP-OES. In further discussions, direct precipitate collection implies the collection of solid through filtration of the crystallizing liquor. In the case of precipitate collection versus ICP-OES significant variations in the mass balance were observed. The precipitate collection values were mostly lower than what the ICP-OES measurements suggested it should be.

The mass balance over calcium can be obtained as $[Ca^{2+}_{inlet}] = [Ca^{2+}_{permeate}] + [Ca^{2+}_{precipitate}]$. In the case of precipitate collection, we can obtain $[Ca^{2+}_{precipitate}]$ directly by actual precipitate collection and in the case of ICP-OES we know $[Ca^{2+}_{permeate}]$ and then $[Ca^{2+}_{precipitate}]$ can be calculated as we know the inlet concentration of calcium $[Ca^{2+}_{inlet}]$. As per our solution preparation scheme, $[Ca^{2+}_{inlet}]$ = 531.89 ppm (mg/L) and at the temperature range the experiments were conducted (~20^0C), the amount of $CaCO_3$ precipitate theoretically predicted at equilibrium is ~470 ppm (0.47 g/L) (refer Figure 2).

Table 10 provides the values for solids precipitated, both in terms of precipitate collection and mass of precipitate obtained from ICP-OES data as Ca^{2+} equivalents. Depletion in supersaturation is expressed as precipitate (obtained via direct precipitate collection or calculated through ICP-OES analysis of permeate) as a percentage of the theoretically predicted amount of solids that

would be precipitated. The precipitate collection is higher when calculated from ICP-OES results when compared to direct precipitate collection. This is explainable by the fact that there some amount of settling of precipitate in the bottom of the reactor and scaling on the walls was observable. Thus, the 'recovery' of precipitate from the mixed liquor through filtration would exclude the crystals that settle and scale the walls of beakers.

Table 10- $CaCO_3$ precipitated.

residence time (τ) (min)	**$CaCO_3$ precipitated (ppm) [solids collected]**	**$CaCO_3$ precipitated (ppm) [ICP-OES]**	**% depletion of supersaturation per [solids collected]**	**% depletion of supersaturation per [ICP-OES]**	**notes**
2.2 ± 0.2	120	236.48	25.5	50.3	(i)
5 ± 0.4	166.67	277.22	35.5	59	(ii)
11 ± 0.5	237.50	308.47	50.5	65.6	(iii)

(i) average of 5 experiments ICP-OES, average of 4 experiments precipitate collection
(ii) average of 2 experiments ICP-OES, average of 2 experiments precipitate collection
(ii) average of 4 experiments ICP-OES, average of 4 experiments precipitate collection

Comparing the depletion rates calculated from the actual precipitate collection and those calculated from the ICP-OES data, it can be observed that as τ increases the difference between percentage depletion obtained from the two methods decreases. It can be conjectured that at lower τ values scaling on beaker walls (heterogeneous crystallization) is significant enough to lower crystal recovery during precipitate collection as the crystals stick to the walls of the CSTRs. In the case of higher τ values scaling appears to less significantly affect precipitate collection due to a lower proportion of crystals sticking to the walls of the CSTRs. At this point it can be speculated that at lower τ values the mechanism of heterogeneous crystallization plays a greater role where the walls of the CSTRs act akin to foreign particulates. While in the case of higher τ values homogeneous

crystallization (crystals growing on crystals) seems to predominate. These conjectures also run counterintuitive to the idea that more homogeneous crystallization could lead to the formation of larger aggregates that can settle faster, thereby reducing the crystal recovery through precipitate collection. However, to conclusively understand the mechanisms discussed above more replicates especially in terms of ICP-OES data are required.

4.5 Influence of aeration on crystallization

Having determined a suitable method to understand the kinetic behavior of $CaCO_3$ crystallization, we proceeded to evaluate the process enhancement making use of hollow fiber membranes (HFM) to introduce bubbles in the CSTRs.

Experiments were carried out to evaluate the effect of air bubbling on crystallization kinetics as discussed in section 2.3.3. Aeration was carried out in two different modes, using an HFM aeration device and the 1/8" tube. The fundamental aim behind using bubbles is to study if the surface area provided by bubbles can act as nucleation sites and if they can enhance crystallization through the route of heterogeneous nucleation. In our conceptualization, we were interested to see if the introduction of bubble surfaces could reduce the induction time for crystallization. In the case of any type of process intervention, it would be most beneficial to look for methods to reduce induction time.

In Figure 22. 'baseline, mixing only' refers to turbidity readings taken when the setup reaches steady state without aeration. After steady state is reached aeration (HFM and plain bubbling) is started and the reactor setup is allowed to reach steady state again. The terms 'after HFM bub.' and 'after plain bub.' refer to turbidity readings taken after steady state is reached when the specific aeration was introduced. The flow rate of air was kept at 10 ± 0.5 mL/min. It can be observed from Figure 22 that aeration does not have any observable effect on crystallization kinetics, as all data

points appear to lie within the same band. This could be because the number density of bubbles in the CSTRs is too low in proportion compared to the amount of crystallizing liquor to affect crystallization significantly. There could also be a possibility that the aeration process does indeed affect the crystallization but the effect is masked by the peristaltic stage which may influence crystallization kinetics much more than the air bubbles.

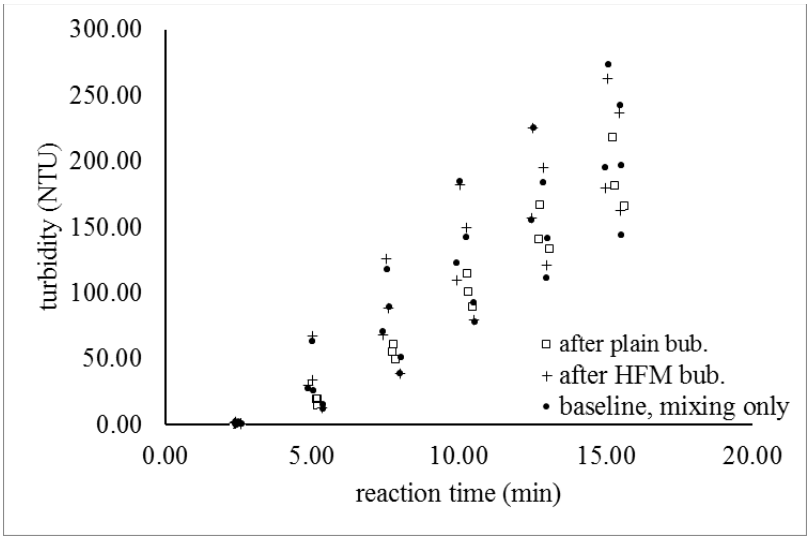

Figure 22- Effect of aeration on crystallization (reaction time vs. turbidity), $\tau \sim 2$ min

Chapter 5

5.1 Conclusions

Batch experiments were carried out to initially analyze crystallization kinetics of sparingly soluble salts ($CaCO_3$) from solutions modelled based on a membrane reject stream. We have developed a novel steady-state-based approach to study crystallization kinetics using a CSTRs-in-series model. We have been able to approximate induction time for crystallizing under this mode of reactor operation. Turbidity has proved to be a useful metric to track the crystallization process. The CSTRs-in-series model has enabled the characterization of induction time for crystallization for a given set of variables viz., τ, impeller action and peristaltic pumping action. We have qualitatively shown the effect of homogenous and non-homogenous nucleation at different levels of the crystallization process by visually analyzing the scaling levels in the different CSTRs corresponding to different levels of reaction time in the series setup. We have also attempted to understand the effect of mixing on the crystallization process by using Kolmogorov length scales. We have developed an explanation in terms of characteristic time for mixing, that brings together microscale mixing and diffusive transport. We have made interesting observations on the effect of peristaltic pumping on crystallization kinetics. The mixing parameters calculated for the CSTRs-in-series model can be used to devise techniques that may be used to scale up to a pellet softener. We have also used ICP-OES and precipitate collection to analyze depletion in supersaturation at various reactor residence times. We were able to devise a steady-state mode of kinetic analysis, and an RTD analysis, which can be adapted to further process modeling to describe dispersion coefficients for coupling mass transfer and crystallization pseudo-reaction kinetics.

Chapter 6

6.1 Future work

6.1.1 More detailed RTD analysis to explore crystallizer behavior

We would like to explore the effect of increasing the rotational speed of the paddle mixer to observe if increased agitation significantly impacts the RTD of the CSTR-in-series setup. More specifically we would like to observe if the agitative effect of increased rotational speed can reduce the dispersion for the overall reactor setup in terms of pulse tracer studies.

6.1.2 Changing model solution supersaturation.

In the present studies, we have used a single type of model solution that precipitates only $CaCO_3$. In future, we plan to use model solutions with a higher concentration of salt but with the same proportion of various ions as in the solution used for the present study. We also plan to use more complex model solutions that are supersaturated with respect to more than one salt.

6.1.3 Patterned surfaces

In the next stage of our work we plan to study the influence of surfaces with regular patterns in nano and microscale on crystallization kinetics. We plan to introduce patterned polymer surfaces inside crystallizers and study its effects on crystallization kinetics. The increase in surface area due to pattern indentation on polymer surfaces could increase the effective surface area available for crystallization. Besides the overall influence of surface area, we are also interested in understanding the surface chemistry of different types of polymers with respect to their interactions with the aqueous phase and the resulting effect on crystallization kinetics. We plan to use a novel type of roll-to-roll imprinting developed by our group to manufacture these patterned surfaces.

6.1.4 Acoustic methods to measure crystallization kinetics

We plan to use piezoelectric transducers to study the properties of crystallizing liquor as crystals emerge in the liquor. We hypothesize that the induction time for crystallization can be more accurately determined by using acoustic/ultrasound-based process monitoring by tracking changes in speed of sound in the crystallizing liquor at various stage of pre-nucleation and nucleation.

6.1.5 Study of mixing processes influencing crystallization

In future, we plan to study the mixing process in tubes in detail**.** We have currently used an algebraic Kolmogorov model to characterize the effect of mixing during the peristaltic stages. This may prove to be an oversimplification; thus, we plan to use low Reynolds number (LRN) k-ε models to characterize the mixing during peristaltic stages.

References

[1] Rosa, S., & Lundager Madsen, H. E. (2011). Kinetics of mass crystallization of calcium carbonate at 25, 30 and 37 c. In Journal of Crystal Growth (Vol. 318, pp. 99–102). https://doi.org/10.1016/j.jcrysgro.2010.11.005

[2] Reddy, M. M., & Nancollas, G. H. (1971). The crystallization of calcium carbonate. I. Isotopic exchange and kinetics. Journal of Colloid and Interface Science, 36(2), 166–172. https://doi.org/10.1016/0022-0248(76)90240-2

[3] Agarwal, P., & Berglund, K. A. (2003). In Situ Monitoring of Calcium Carbonate Polymorphs during Batch Crystallization in the Presence of Polymeric Additives Using Raman Spectroscopy. Crystal Growth and Design, 3(6), 941–946. https://doi.org/10.1021/cg0256125

[4] Wiechers, H. N. S., Sturrock, P., & Marais, G. v R. (1975). Calcium carbonate crystallization kinetics. Water Research, 9(9), 835–845. https://doi.org/10.1016/0043-1354(75)90143-8

[5] Mullin, J. W. (2002). Crystallization, 4th Edition By J. W. Mullin. 2001. Butterworth Heinemann: Oxford, UK. 600 pp. ISBN 075-064-833-3. Organic Process Research & Development, 6(2), 201–202. https://doi.org/10.1021/op0101005

[6] With, G. De, & Sommerdijk, N. A. J. M. (2009). CaCO 3 Formation Revealed by Cryo-TEM. science (Vol. 587).

[7] Pouget, E. M., Bomans, P. H. H., Goos, J. A. C. M., Frederik, P. M., de With, G., & Sommerdijk, N. A. J. M. (2009). The Initial Stages of Template-Controlled CaCO3 Formation Revealed by Cryo-TEM. Science, 323(5920), 1455–1458. https://doi.org/10.1126/science.1169434

[8] Rieger, J., Frechen, T., Cox, G., Heckmann, W., Schmidt, C., & Thieme, J. (2007). Precursor structures in the crystallization/precipitation processes of CaCO3 and control of particle formation by polyelectrolytes. Faraday Discussions, 136, 265-277. https://doi.org/10.1039/b701450c

[9] Gebauer, D., Völkel, A., & Cölfen, H. (2008). Stable prenucleation calcium carbonate clusters. Science (New York, N.Y.), 322(5909), 1819–22. https://doi.org/10.1126/science.1164271

[10] Lam, R. S. K., Charnock, J. M., Lennie, A., & Meldrum, F. C. (2007). Synthesis-dependant structural variations in amorphous calcium carbonate. CrystEngComm, 9(12), 1226–1236. https://doi.org/10.1039/b710895h

[11] van Schagen, K., Rietveld, L., Babuška, R., & Baars, E. (2008). Control of the fluidised bed in the pellet softening process. Chemical Engineering Science, 63(5), 1390–1400. https://doi.org/10.1016/j.ces.2007.07.027

[12] McCool, B. C., Rahardianto, A., Faria, J. I., & Cohen, Y. (2013). Evaluation of chemically-enhanced seeded precipitation of RO concentrate for high recovery desalting of high salinity brackish water. Desalination, 317, 116–126. https://doi.org/10.1016/j.desal.2013.01.010

[13] Chong, T. H., & Sheikholeslami, R. (2001). Thermodynamics and kinetics for mixed calcium carbonate and calcium sulfate precipitation. Chemical Engineering Science, 56(18), 5391–5400. https://doi.org/10.1016/S0009-2509(01)00237-8

[14] Pellegrino, J. (2017). Concentrate stream management with pellet softening,11th Quarter report (Bureau of Reclamation Cooperative Agreement No. R14AC0075), Master Cooperative Agreement, Rocky Mountains Cooperative Ecosystem Studies Unit, Document Number: 06AG602112. (unpublished)

[15] Garside, J., & Shah, M. B. (1980). Crystallization Kinetics from MSMPR Crystallizers. Industrial and Engineering Chemistry, 19(2), 509–514. https://doi.org/10.1021/i260076a001

[16] Hostomsky, J., & Jones, a G. (1991). Calcium carbonate crystallization, agglomeration and form during continuous precipitation from solution. Journal of Physics D: Applied Physics, 24(2), 165–170. https://doi.org/10.1088/0022-3727/24/2/012

[17] Powell, K. A., Saleemi, A. N., Rielly, C. D., & Nagy, Z. K. (2015). Periodic steady-state flow crystallization of a pharmaceutical drug using MSMPR operation. Chemical Engineering and Processing: Process Intensification, 97, 195–212. https://doi.org/10.1016/j.cep.2015.01.002

[18] Machej, K. (1994). Crystal growth dispersion in an MSMPR crystallizer - a mathematical model. Chemical Engineering and Processing, 33(6), 465–468. https://doi.org/10.1016/0255-2701(94)80002-2

[19] Li, J., Trout, B. L., & Myerson, A. S. (2016). Multistage Continuous Mixed-Suspension, Mixed-Product Removal (MSMPR) Crystallization with Solids Recycle. Organic Process Research and Development, 20(2), 510–516. https://doi.org/10.1021/acs.oprd.5b00306

[20] Fogler, H. S. (2006). Elements of chemical reaction engineering. Prentice Hall PTR International Series in the Physical and Chemical Engineering Sciences, 4th, 1080. https://doi.org/10.1016/0009-2509(87)80130-6

[21] Mersmann, A. (1995). Crystallization Technology Handbook. 2nd Edition (Vol. 13). https://doi.org/10.1080/07373939508917003

[22] Segev, R., Hasson, D., & Semiat, R. (2011). Improved high recovery brackish water desalination process based on fluidized bed air stripping. Desalination, 281(1), 75–79. https://doi.org/10.1016/j.desal.2011.07.043

[23] Segev, R., Hasson, D., & Semiat, R. (2013). Modeling CaCO3 precipitation in fluidized bed CO2 stripping desalination process. Desalination, 311, 192–197. https://doi.org/10.1016/j.desal.2012.11.024

[24] Joanes, D. N., & Gill, C. A. (1998). Comparing measures of sample skewness and kurtosis. Journal of the Royal Statistical Society: Series D (The Statistician), 47(1), 183–189. https://doi.org/10.1111/1467-9884.00122

[25] Paul, Edward L. Atiemo-Obeng, Victor A. Kresta, Suzanne M.. (2004). Handbook of Industrial Mixing - Science and Practice. John Wiley & Sons. Online version available at: http://app.knovel.com/hotlink/toc/id:kpHIMSP001/handbook-industrial-mixing/handbook-industrial-mixing

[26] Furukawa, H., Kato, Y., Inoue, Y., Kato, T., Tada, Y., & Hashimoto, S. (2012). Correlation of power consumption for several kinds of mixing impellers. International Journal of Chemical Engineering. https://doi.org/10.1155/2012/106496

[27] Raju, K. S.. "Chapter 3 - Piping, Seals, and Valves". Fluid Mechanics, Heat Transfer, and Mass Transfer: Chemical Engineering Practice. John Wiley & Sons (2011). Books24x7. http://common.books24x7.com.colorado.idm.oclc.org/toc.aspx?bookid=40660 (accessed June 30, 2017)

[28] Saleh, J. M., & Saleh, J. M. (2002). 31.9. The Measurement of Turbulence. In Fluid flow handbook. New York: McGraw-Hill.

[29] Ruzicka, M. C. (2008). On dimensionless numbers. Chemical Engineering Research and Design. https://doi.org/10.1016/j.cherd.2008.03.007

[30] Li, Y. H., & Gregory, S. (1974). Diffusion of Ions in Sea-Water and In Deep-Sea Sediments. Geochimica et Cosmochimica Acta, 38(June), 703–714. https://doi.org/10.1016/0016-7037(74)90145-8

[31]Kleizen, H. H., de Putter, A. B., van der Beek, M., & Huynink, S. J. (1995). Particle concentration, size and turbidity. *Filtration and Separation*, *32*(9), 897–901. https://doi.org/10.1016/S0015-1882(97)84175-4

List of acronyms

ICD= intermediate concentrate treatment

HFM= hollow fiber membrane

NTU= nephelometric turbidity units

DI= deionized

CSTR= completely stirred tank reactor

RTD= residence time distribution

C(t)= function of concentration with respect to time

E(t)= exit age distribution

t_m= cumulative mean residence time

t= time associated with residence time distribution

σ= standard deviation associated with residence time distribution

σ^2= variance associated with residence time distribution

V= volume of each reactor

v_o= volumetric flow rate to reactor

τ= residence time in one completely stirred tank reactor

t_s= stabilization time for one completely stirred tank reactor

k= first order reaction rate constant

Δt= small time in which pulse input is inputted

n= number of elements in the population

x_i = individual element of the population

$\bar{x}$ = mean

s_1= skewness

s_0= bias corrected skewness

A_T= area of each completely stirred tank reactor

Re_{Im}= Reynolds number of impeller

N_p= Newton number

N_{Im}= rotational speed of impeller

ρ= density of water

μ= dynamic viscosity of water

M_{CSTR}= mass of liquor in each completely stirred tank reactor

ν= kinematic viscosity of water

D_{Im}= diameter of impeller

P_{Im}= impeller power

ε_{Im}= impeller dissipation

u_{avg}= average velocity of liquid in peristaltic tube

q= volumetric flow rate in peristaltic tube

Δp= pressure drop in peristaltic tube

f_D= Darcy friction factor

Re= Reynolds number in peristaltic tube

D= diameter in peristaltic tube

L= length of peristaltic tube

P_{tube}= power for pumping in peristaltic tube

ε_{tube}= dissipation in peristaltic tube

V_c= volume in peristaltic tube per second

ε_{tot}= total power dissipation due to peristaltic pumping and impeller action

η= Kolmogorov mixing length scale

D_a= diffusivity of Ca^{2+}

t_c= characteristic time

Da_{II}= Damkohler number of the second type.

F_o= Fourier number

LRN= low Reynolds number

Appendix

A. CSTRs-in-series

Framework of CSTR-in-series experiments

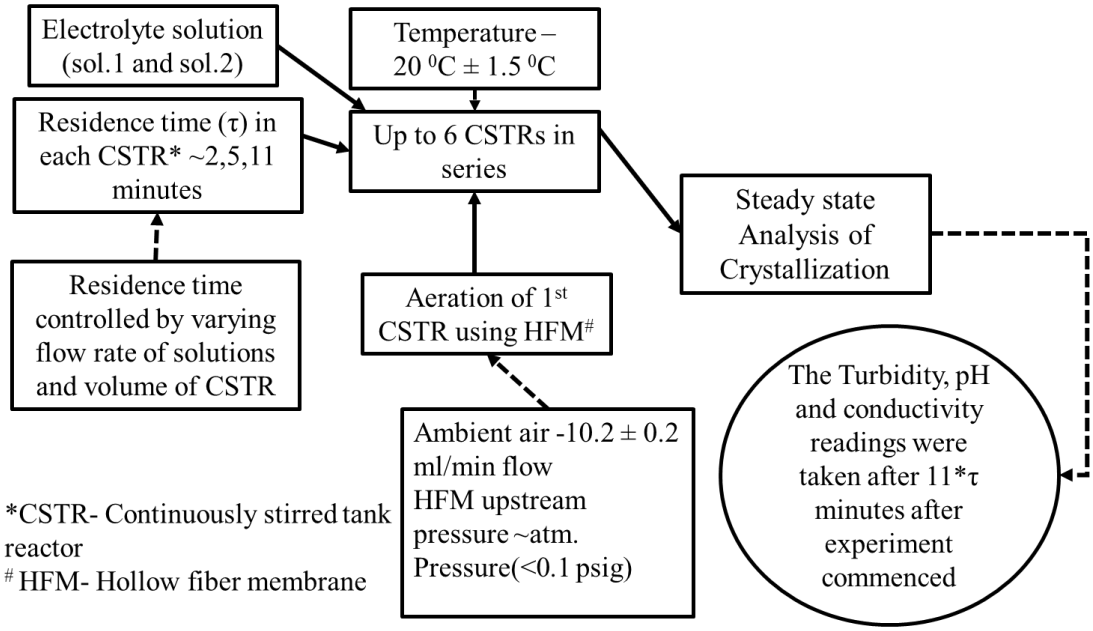

Figure A1- Overview of the Steady state experimental setup

Nephelometric turbidity units (NTU)

Turbidity or extent suspend particles in solution can be measured by measuring light interactions with suspended particles. In our experiments, we have used a single detector tungsten lamp light source with a peak wavelength in the 400-600 nm region. Besides the actual number of particles that cause scattering the particle size also determines the scattering. Based on the size of the particle (d_p) and the wavelength of light (λ) used, the scattering can be either Rayleigh ($d_p/\lambda \leq 0.05$), Mie ($d_p \sim \lambda$) or Fraunhofer ($\lambda / d_p \leq 0.05$) [31].

Cleaning of reactor setup

The cleaning of reactor setups was carried out using 4% hydrochloric acid (HCl). The reactor setup, including tubing was cleaned with an acidic solution to remove the deposition of crystals. We had to be careful with the cleaning process as any remaining HCl in the system could affect

the pH and ultimately affect the crystallization process. This was especially a problem with the peristaltic pump tubing. Thus, we evolved a reliable protocol to clean the tubes. The tubes were first pumped with a 4% solution of HCl and then tap water was pumped through the tubing followed by DI water. The tubing was pumped with DI water till the time the outlet DI water had a conductivity of less than ~ 10 μS/cm. This made sure that we did not get any interference due to the HCl used for cleaning the tubing.

B. Challenges in experimental methodology

Air supply

One of the main challenges in performing aeration experiments as discussed in Chapter 1 was the difficulty in ensuring exact molar flow rates of air to the jars. Initially we were attempting to partition air from a single header to different jars by manipulating valves and ensuring a similar back pressure across portioned lines. This proved to be a difficult task. We started using peristaltic pumps with multiple pump heads mounted onto a single drive to ensure exact molar air flow rates to jars. This method also enabled easier air flow control besides being able to supply similar molar flows to different jars.

Solution preparation

In terms of experimental techniques, there were quite a few challenges that were faced. In the case of electrolyte preparation, our methodology was to prepare the solutions in a concentrated form followed by dilution in large volumes of water (~ 50 liters) to obtain the requisite levels of concentrations. If the solutions are not rapidly mixed before the start of experiments, certain undissolved salt particulates and density stratification created due to improper mixing resulted in changing electrolyte composition while performing the experiment. That is, the inflow of concentration into the reactor setup was not uniform. We overcame this difficulty by mixing the electrolytes rapidly using a paint mixer actuated by a drill before each experiment.

Bubbling through level control tubing

As mentioned in earlier sections we ran the peristaltic pumps when transferred the crystallizing liquid between reactors at a higher flow rate than required. This resulted in a situation where the tubes were pumping in air into the crystallizing solution resulting in the introduction of bubbles. This was a problem because we were attempting the see if the small number of bubbles that we

were introducing into the system had any effect on crystallization metrics. Excessive bubbling was created in the crystallizing solution due to the pumps running at higher speeds than required to pump the fluid. The pumps were required to be run at a higher speed than required to be certain of accurate level control in the CSTRs. Thus, bubbling through level control could possibly crowd out the effect of aeration based process interventions. We resolved this issue by making sure that the ‘drop ends’ of the tubing do not come in contact with the solution. The tubing was directed to face the wall of the reactor so that the air in the tubing does not cause bubbling in the crystallizing liquor.